Cosmic gamma ray bursts, its parameters and correlations

Jana Poledniková

Diploma thesis
supervised by assoc. prof. René Hudec Ph.D.

2011

Department of Theoretical Physics and Astrophysics
Faculty of Science
Masaryk University

I declare that I wrote my diploma thesis independently and exclusively using sources cited. I agree with borrowing the work and its publishing.

In Brno, May 13 2011 Jana Poledniková

My thanks belong to my supervisor René Hudec who made this work possible. I would also like to thank people from the Swift Mission Operations Center, especially prof. John Nousek, who provided many interesting remarks and ideas and also Kim Page from Swift UK team in Leicester who taught me everything about the Swift data analysis.

And in the end, I want to thank my supportive family and to my friends, šnEk who helped the first lines to happen and Ondrej who was a huge support for the typesetting.

Acknowledgement

This diploma thesis was supported by grants GA ČR 102/09/0997 and ESA PECS C98023.

Typographic note

The `typewrited` text is used to describe programs, scripts, webpages and the direct outcomes of the scripts.

Acronyms

Below is the list of the most frequent acronyms used in the work.

GRB gamma-ray burst. With number, it refers to a concrete burst GRByymmdd, where yy stands for a year, mm for a month and dd for a day. If more than one gamma ray bursts are observed during the day, letters A,B, ... are used to distinguish them.
BAT Burst Alert Telescope onboard Swift satellite.
XRT X-Ray Telescope onboard Swift satellite.
UVOT Ultra-Violet Optical Telescope onboard Swift satellite.
CGRO Compton Gamma-Ray Observatory.
BATSE Burst And Transient Source Experiment onboard CGRO.
S/N signal to noise ratio.
MET Mission Elapsed Time.

If not mentioned otherwise, the cgs unit system is used.

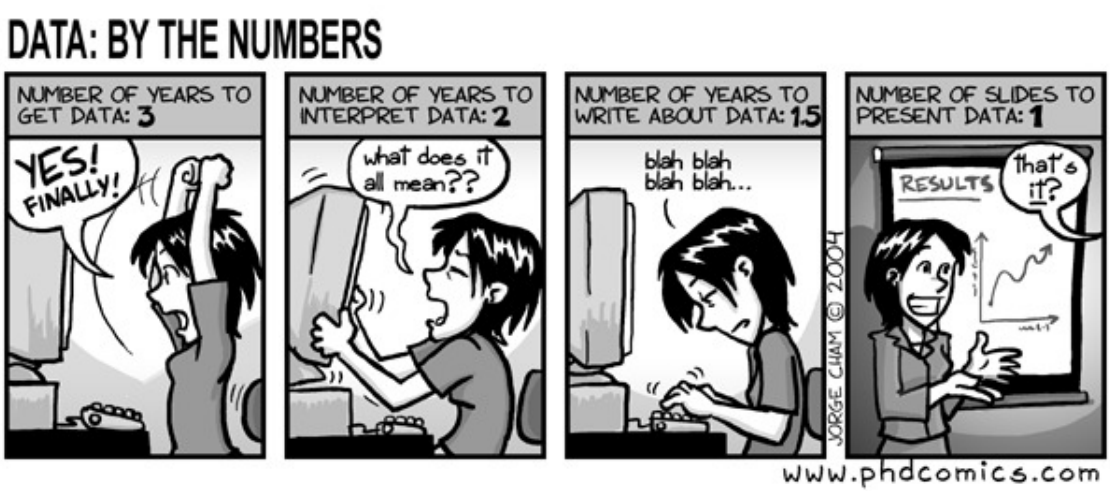

May the force be with you!

– Star Wars

Abstract:

The work is dedicated to the study of the most energetic phenomena in the whole Universe, to gamma-ray burst. It provides short overview of the knowledge concerning this events. It deals with the data from the Swift satellite which provided the biggest number of the bursts with known redshifts. A brief overview of the data analysis is also given so the technical part of this work can be used as a manual to process Swift data. Since only the prompt emission, not the afterglow, is considered, the data are taken from the BAT instrument onboard Swift satellite. A new approach dealing with the geometrical features in the light curves is introduced for classifying the gamma light curves. The major outcome is that within the groups, some weak correlation can be found, but without clear physical meaning. In general, the correlation within the whole sample are mostly nonexisting, as was assumed in the earlier works. Though the earlier proposed correlations dealing with the same parameters were confirmed.

Keywords: gamma-rays: bursts - gamma-rays: observations

Contents

1 Introduction

The easiest way to describe a gamma ray burst is to say that it is the most energetic explosion in the whole Universe. And in fact this description is probably the most used one. Explaining such phenomena is not easy and it is still quite far from being properly described using mathematical models. The first part of this work briefly introduces the history of the search for the gamma-ray bursts and the first achievements. The basics of one of the most accepted model are discussed. The model is not discussed in a great detail, since it is not an aim of this work. Other models are not discussed at all since they are often disproved. If I can paraphrase one famous quote 'Never run after a bus or woman or a gamma-ray burst theory, because therell always be another one in a few minutes.' In general this statement can cover the whole field concerning this high energy phenomena.

Most informations known about the gamma ray bursts are the outcomes of the observational and statistical studies. Since the progenitor is fain before the burst occurs and is probably completely destroyed afterwards[1], all we can do is to look at the environment and try to estimate at least some informations and parameters. This thesis deals with the topic in the same, statistical and observational, way. Hence the second part deals with the observations and can be used as a simple manual to analyze Swift data. The data are obtained from the Swift satellite because of the good data accessibility and general fruitfulness of the mission. It makes Swift salient in between all the other gamma-ray burst mission. Since the Swift satellite is such a celebrity amongst gamma-ray missions, it is also briefly discussed from the technical point of view. In general, if there is no way to improve the theory, the only thing one can do is improve the technology. The last part of the work is aimed on the conclusions. A new approach dealing with

[1]Thought some studies searching for the gamma-ray burst remnant were introduced.

the geometrical features in the light curves is proposed and the parameters and their correlations are explored from the new point of view.

By all means, the mystery of the gamma ray burst is apparently not to be uncovered in this work and possibly not in the near future. This phenomena just provides a perfect sandbox for the imagination and creativity.

2

The Tale of Discovery

Gamma-ray bursts (GRBs) may be called a side effect of the Cold war. If it wasn't for the Cold war and monitoring of the nuclear tests, we probably wouldn't notice those flashes of gamma-rays at all. The first serendipitous observation was made on July 2, 1967 by the US Vela satellites [58].

Vela (a Spanish word for 'a watch') satellites were launched to the orbit in early 60's to monitor imprints of the nuclear bomb testing. Those tests were forbidden by Nuclear Test Ban Treaty from 1963. But US army was suspecting that the Soviet Union will continue the tests despite of the pact. The first satellite was launched in 1963, one week after the Nuclear Test Ban Treaty was signed, the last one was launched in 1970. The orbit of the satellites was 105,000 km above the Earth surface (most satellites orbited at an altitude of 800 km). This altitude was favorable in two ways – the orbit was above the van Allen radiation belt, what reduced the noise caused by high energy particles in the Earth's magnetic field, and the height of the orbit allowed satellites to observe behind the Moon, where the Americans expected Soviets to conduct the testing.

On July 2, 1967, at 14:19 UTC Vela 4 and Vela 3 detected something very strange. A typical signature of the nuclear explosion would be roughly millionth of a second lasting intense flash and steady fading thanks to nuclear decay. The detection from July 2 was different, it didn't bear any of the mentioned imprints. The light curve of the event showed a double peaked structure without the decay imprint. This was something peculiar but since the project was conducted by the US army, the data were classified for some time and were put into an archive for further investigation.

On May 23, 1969, Vela 5 satellite was launched. For the first time, the team in Los Alamos National Laboratory focused not only on the signature

of the nuclear testing[1], but also on strange gamma-ray bursts. Shortly after the launch, there were twelve detections of an unknown origin. The team suspected that the gamma ray bursts come from supernovae or from Solar flares. But for those twelve detections, there were neither corresponding supernovae nor Solar flares observations. Some of the burst showed the same double peaked structure at the one from July 2. On April 18, 1970, another Vela satellite (Vela 6) was launched with intention to determine where the gamma-ray burst come from. In order to determine the location on the sky, the team wanted the satellites to be as far away from each other as possible. The distance between them was 10,000 km. This distance allowed to watch the signal with a time difference between both satellites which enabled the back-tracing the direction of the burst. It was concluded that the bursts do not origin anywhere in the Solar system.

In the years 1969 - 1972, total number of sixteen gamma ray bursts not connected to the supernovae or Solar flares, were observed. Those finding were published in [29]. The observed bursts had energies ranging between $0.2 - 1.5$ MeV (the upper level is constrained due to the sensitivity of the detectors onboard), duration was $0.1 - 30$ s and integrated flux densities $\sim 10^{-5} - 2 \cdot 10^{-4} \mathrm{erg} \cdot \mathrm{cm}^{-2}$.

However it was stated that the GRBs do not originate in the Solar system, it was still unclear, if they are galactic or extragalactic. Also the mechanism producing such energetic bursts was still a mystery.

[1]There was not a single detection of the nuclear weapons testing in the history of the project.

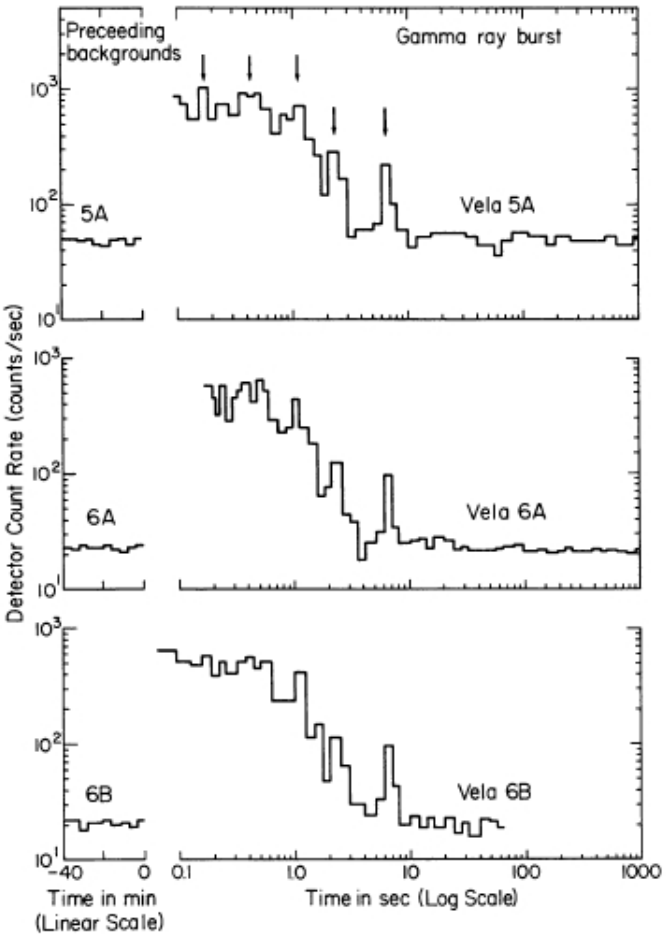

Figure 2.1: One of the first GRB detection from August 22, 1970. The preceeding background is the count rate before the detection. Arrows point to some common features. Count rates have been reduced by 100 counts per second [29].

3
Bimodal distribution

By the time, Vela project ended, there was no satellite to observe the sky in gamma-rays. The first successor in this field was Compton Gamma Ray Observatory (CGRO) with Burst And Transient Source Experiment (BATSE) onboard. This experiment was dedicated solely to the transient sources and could even estimate the location of the burst. Since there were way more questions than answers in this field, there were a big expectations laid out for this mission.

3.1 Brief description of the experiment

The CRGO project [67] lasted nine years (1991 - 2000). CRGO was able to monitor the sky in unprecedentedly wide spectrum - 30 keV – 30 GeV. There were four instruments onboard. The Burst And Transient Source Experiment (BATSE), the Oriented Scintillation Spectrometer Experiment (OSSE), the Imaging Compton Telescope (COMPTEL), and the Energetic Gamma Ray Experiment Telescope (EGRET). A brief description of the instruments is provided below.

BATSE was an all sky monitor. To cover all the sky, there were total number of eight detectors, one at every corner of the observatory. The detectors were simple NaI crystals that produced a flash of light while exposured to the gamma-rays. Those flashes were digitalized and the energy and duration of the GRB were computed. The detectors were sensitive from 20 keV to several GeV.

OSSE consisted of four NaI scintillation detectors. The sensitivity range was 50 keV - 10 MeV. Every detector could have been pointed individually. It mostly allowed the subtraction of the background for the detected GRBs. The detector was used mostly for study of the Solar flares and supernova remnants.

COMPTEL was an imaging telescope suitable for energies 1 eV - 3 MeV. It consisted of two scintillating detectors, one was liquid and the other, lower, one was NaI detector. The instrument recorded the time, location, and energy of the events in each layer of detectors. This feature enabled determination of the direction and energy of the original gamma-ray photons and reconstruction of an image and energy spectrum of the source.

EGRET covered the most energetic energy bands detectable with CGRO. The energy range was 20 MeV - 30 GeV. It consisted of a spark chamber, where electron - positron pairs were produced, and th NaI detector. The path of the incoming photons was measured and then the direction of the original GRB was computed. This instrument was also able to estimate the energy of the burst.

3.2 First CGRO success – isotropic distribution

Short after the discovery of the GRBs, it was clear that they do not originate in the Solar system, however it was very unclear if they are galactic or extragalactic. To determine the origin, one should know the distance of the GRB, or the areal distributions of them. One of the first theories stated that gamma ray bursts originate in the neutron stars [13]. If this theory would be right, all the GRBs should be clustered along the galactic plane. Despite Vela's ability to determine the location of the burst, the sample was too small for the statistics. Since CGRO was designed especially to catch the GRBs, it was expected that there will be more results. In the end, there were 2704 bursts, isotropically distributed over the sky [67].

Isotropic distribution ruled out the possible origin in the galactic neutron stars. The isotropic distribution of the GRBs was proposed for the first time by the KONUS data [40] and was in fact confirmed by the CGRO since BATSE caught many more bursts [9]. But it didn't rule out other possibilities within our galaxy. The only way to prove that GRBs are extragalactic is

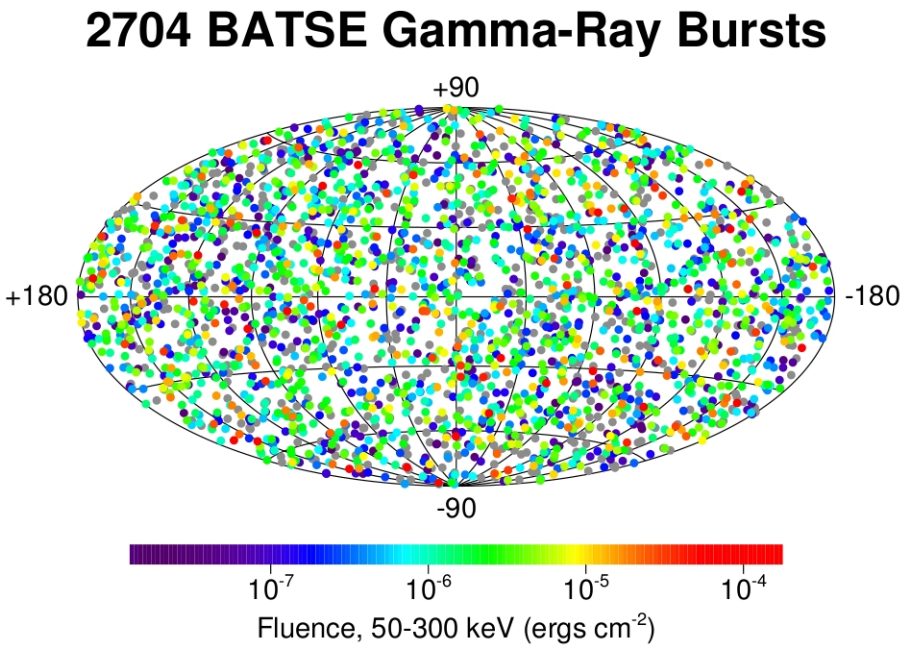

Figure 3.1: Distribution of GRBs detected by BATSE onboar CGRO on the sky. Courtesy of NASA.

to measure the distance. For this, detection of the afterglow[1] is needed. CGRO wasn't equipped with anything to detect them, so the discovery of the first afterglow was left for satellite called BeppoSAX (Beppo was an Italian physicist, SAX stands for Satellite for X-ray astronomy), in February 28, 1997 [16].

[1]Detection of the transient source in the other energy bands.

3.3 Bimodal distribution

One of the biggest success of the CGRO is discovery of the bimodal distribution. As was mentioned before, CRGO was able to detect a big number of the bursts. The first BATSE catalogue consisted of 260 bursts. It was enough for global analysis. Parameters that were used for this study were T_{90} and T_{50} [31]. These parameters are related to the durations of the bursts. T_{90} is defined as the time interval over which 90% of the total background-subtracted counts are observed, with the interval starting when 5% of the total counts have been observed. T_{50} is defined analogically, thought at present times, T_{90} is used in most cases. The counts used for the BATSE study had to be > 25 keV. The graphs below from [33] show the distribution of the durations.

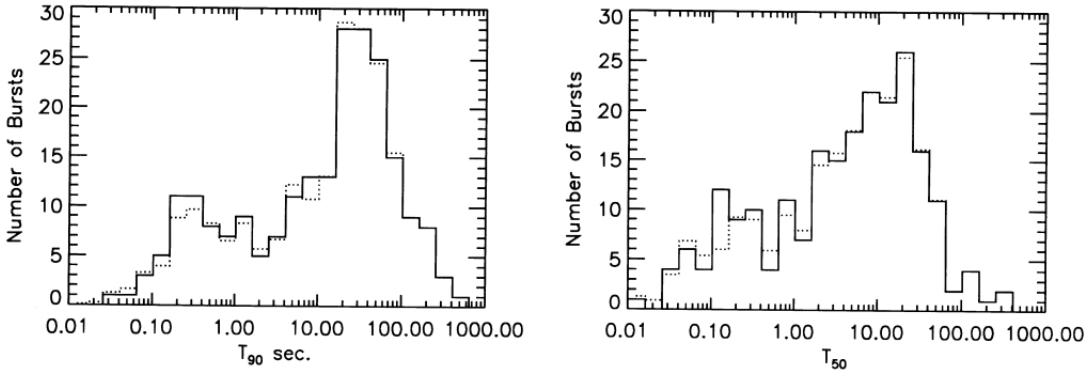

Figure 3.2: Bimodal distribution of the first 222 BATSE GRBs. The left graph shows the distribution for T_{90}, the right graph shows the distribution for T_{50}. From [33].

There is a dip around two seconds. This basically divided observed GRBs into two subsets [33] which were proposed for the first time by the results from KONUS experiment onboard Venera spacecrafts[40]. Long gamma ray bursts with duration longer than 2 seconds, short gamma ray bursts with duration shorter than two seconds. Both classes of the GRBs were tested for the isotropic distribution and both classes agreed with the previously assumed isotropy. Soon after the discovery of those two groups, it was also established that the long GRBs tend to have soft spectrum whereas the short ones have hard spectrum [33]. This was also confirmed by the data

from Phebus experiment onboard Granat mission [36].

In the recent studies, the third group of GRBs with intermediate duration $T_{90} \sim 2$ s was proposed [27]. Nevertheless the existence of this group causes dubiousness in the community and it is still not fully confirmed.

4
Little bit of theory

The theory concerning the GRBs could by described as a bit blurry. Below mentioned model is the most succesful, however it is not able to describe all the observable features in the GRBs. In general all the models rely on the relativistic numerical simulations of the magnetohydrodynamics. Since the modeling was not the aim of this work, the theory will not go into the details.

The below described theory of the GRBs is relativistis fireball shock model which is able to create a strongly beamed jet, proposed by [48][50]. The model is able to explain many features of the GRB, however not all of them.

GRBs are huge explosions in the cosmological distances. The fluxes imply that the energy released in the burst is $\leq 10^{54}$ erg. It is estimated the emission is isotropic. In order not to disturb causality, this energy has to be released in a region ≤ 100 km on less than few seconds (or even less) timescales. Such explosion imply formation of a relativistic gamma firebal and electon-positron pair, which will expand relativisticaly [12][45]. The relativistic outflow is strongly supported by the fact that the observed photons have energies $\epsilon \gg 0.5$ MeV [20]. This is because in this case the relative angle at which the photons collide must be less than the inverse of the bulk Lorentz factor Γ^{-1} and the effective threshold energy for pair production is correspondingly reduced. Roughly, the Lorentz factor must satisfy

$$\Gamma \geq 10^2 \left(\frac{\epsilon_\gamma}{10\mathrm{GeV}}\right)^{1/2} \left(\frac{\epsilon_t}{10\mathrm{MeV}}\right)^{1/2}, \tag{4.1}$$

if this condidion is fulfilled, photons $\epsilon_\gamma \geq 10$ GeV will escape anihilation against target photons with $\epsilon_t \sim 1$ MeV. This calculation is further described in [38].

In general we can link relativistic energy and the mass

$$M_0 \ll \frac{E_0}{c^2}. \tag{4.2}$$

This mass has to be released from a radius r_l. Expansion follows as the gas converts its internal energy into bulk kinetic energy. From this, we can write

$$\Gamma \simeq \frac{r}{r_l} \propto r. \tag{4.3}$$

Comoving temperature drops $\propto r^{-1}$. Another constraint is placed on the Lorentz factor,

$$\Gamma_{max} \sim \eta \sim \frac{E_0}{M_0 c^2}. \tag{4.4}$$

This is a simple outline of the model, nevertheless not sufficent. In order to explain some more of the GRB physics and to be consistent with the observations, one must employ more ideas. Among these are that the expansion of the fireball should lead to a conversion of most of its internal energy into kinetic energy of the released baryons, rather than into photon luminosity, hence it would be energetically very ineficient. Furthermore, it would produce a quasi-thermal photon spectrum, instead of the observed power-law spectra. This can be explained using external [48] and internal[50] fireball shock model.

4.1 External shock

External shock[49] will occur every time in any outflow of the total energy E_0. Let's assume average particle density n_0, then for the radius and the timescale

$$r \sim 10^{17} E_{53}^{1/2} n_0^{-1/3} \eta_2^{-2/3} \mathrm{cm}, \tag{4.5}$$

$$r \sim \frac{r}{c\Gamma^2} \sim 3 \times 10^2 E_{53}^{1/3} n_0^{-2/3} \eta_2^{-8/3} \mathrm{s}. \tag{4.6}$$

The lab frame energy of the external matter ($\Gamma^2 m_p c^2$) equals the initial energy E_0 of the fireball. This model is able to explain observational features

i.e. synchrotron spectra. External shock is even able to explain the afterglow radiation. The observer-frame dynamic time is

$$t \sim \frac{r}{c\Gamma^2} \sim t_{\rm burst} \sim \text{seconds}. \tag{4.7}$$

External shock is able to explain multiple peaks [46], therefore this scenario is able to explain long, smooth bursts.

4.2 Internal shock

Internal shock, as proposed in[50] is on the other hand able to explain the variability in the lightcurves. This model has to deal with the fact that in order to obtain variable lightcurve, one has to have a central engine which is able to eject energy at a variable rate [20]. In general, the internal shock model leads to successive shells ejected with different Lorentz factor. Faster shells will overtake the slower ones, hence the shock is interacting with itself. The central engine outflow can be taken as a wind of duration t_w. Significant variations of order $\Delta\Gamma \sim \Gamma \sim \eta$ occuring on the timescales $t_{var} \ll t_w$, where t_{var} stands for the time of variations, will lead to the internal shocks at radii r_{dis} above the so called Compton photosphere r_{phot}.

$$r_{dis} \sim c t_{var} \eta^2 \sim 3 \times 10^{14} t_{var} \eta_2^2 \text{cm}, \tag{4.8}$$

$$r_{phot} \sim \frac{\dot{M}\sigma_T}{4\pi m_p c \eta^2} \sim 10^{11} L_{50} \eta_2^{-3} \text{cm}. \tag{4.9}$$

In this scenario, most of the energy comes out in the form of shocks. The variations can be produced also above the photosphere on the timescales

$$t_{var} \geq t_{var,min} \sim 10^{-3} \left(\frac{M_c}{M_\odot}\right)^{2/3}, \tag{4.10}$$

where M_c stands for a central object mass. This is valid for an outflow originating in a central object of mass M_c at radii $\geq r_0 \sim c t_{var.min}/2\pi$.

Internal shock is able to explain complicated lighcurves with variations on the milisecond scale. This scenario vas mostly able to explain even very complicated lightcurves [30][17].

4.3 Brief overview

In general, GRB is a relativistic outflow collimated within some jet of solid angle $\Omega_j < 4\pi$. It is assumed that the observer must be in the line of sight and $\Gamma \geq \Omega_j^{-1/2}$[43], hence the light cone is inside the jet boundary. As the velocity of the material in the jet decelerates, the Lorentz factor drops and changes in the lightcurve will occur. It is believed that the internal shock occurs and is followed by the external shock [50] - the internal-external shock scenario. The external shock consists of forward shock moving into the external medium and reverse shock moving backwards into the ejecta, decelerated by the medium. Internal shock is believed to be more symmetrical in the nature.

5
Morphology and correlations

Soon after the discovery, the first attempts to classify the morphology and the periodicity of the light curves were made. It was a natural step since this approach was quite successful in history (i.e. classification of the supernovae [18] or periodicity of the variable stars i.e. [34]). Very early, it was discovered that the GRB light curves differ in the terms of both, timescales as well as shapes. There were various attempts to classify GRBs using these. As was mentioned in the Chapter 3, bimodal distribution and two classes of the GRBs were proposed according to the duration and hardness. The attempts to classify GRBs according to morphology and the known relations are discussed further.

5.1 Morphology

The first attempts to classify GRBs according to the light curves morphology were done by dealing with the periodicity. A big fraction of the GRBs display multiple peaks, which were believed to exhibit periodic behavior. Unfortunately in general, these studies proved to be unsuccessful. However there were some results i.e. a 2.2 s periodicity was found in the GRB840804 observed by Solar Maximum Mission (SMM) [32] or a display of a 5 second lasting quiet phase between two peaks detected in seven events within the KONUS data [41]. Later, it was proposed that the events displaying periodicity were different in nature and form a new class of the objects, known as soft gamma repeaters (SGR) [13] [14].

More attempts were made with a bigger number of detection, however in the CGRO times, it was established that no gamma-ray burst light curves are alike. There were several attempts to establish groups amongst GRBs

according to the morphology of the curve. The most successful one was a model called Fast Rise Exponential Decay (FRED). The light curve exhibited short steep rise and long fading [19]. Unfortunately this class didn't provide any insights into the nature of the GRBs.

More studies were dedicated to the study of the widths of the light curves. Amongst them a study of the spikiness [37]. Based on the parameter which described spikiness of the burst, there was no indication for two groups of GRBs. Another quite successful study showed that several parameters (rise and decay times, FWHM of the pulses and separation between pulses) exhibit log-normal distribution [55][56][57][5].

The behavior of the gamma-ray light curves is still not clearly explained, since it looks like every GRB has its own imprint which is dependend on many factors, i.e. environment of the burst or the mechanism of the shock waves [50]. There were many studies dedicated to the morphology but mostly unsuccessful [19], since they usually failed to explain more than one burst, so they will not be discussed there.

5.2 Known correlations

Search for the correlations within the gamma-ray bursts is like a search for a Holy Grail. Everybody want to find some sort of correlation. One of the first successful discoveries was the hardness-duration correlation [33][36]. The era of looking for correlations within GRBs reached its golden age by the discovery of the afterglows and possibility to estimate the distances. The correlations listed below belong to the most significant ones in the field. The correlations that proved to be wrong or not significant will not be discussed in the text.

5.2.1 Amati relation

After the group of the GRBs with measured redshifts grew bigger, first studies were performed. One of them deals with the relation between the peak energy (E_{peak}) and isotropic energy (E_{iso})[1][1]. E_{iso} is the total energy radiated by the GRB during its prompt phase. The whole study was dedicated to a group of twelve GRBs where several correlations were proposed, however the most

[1]In the original work, it was called E_{rad}, but nowadays the community agrees on calling the parameter E_{iso}.

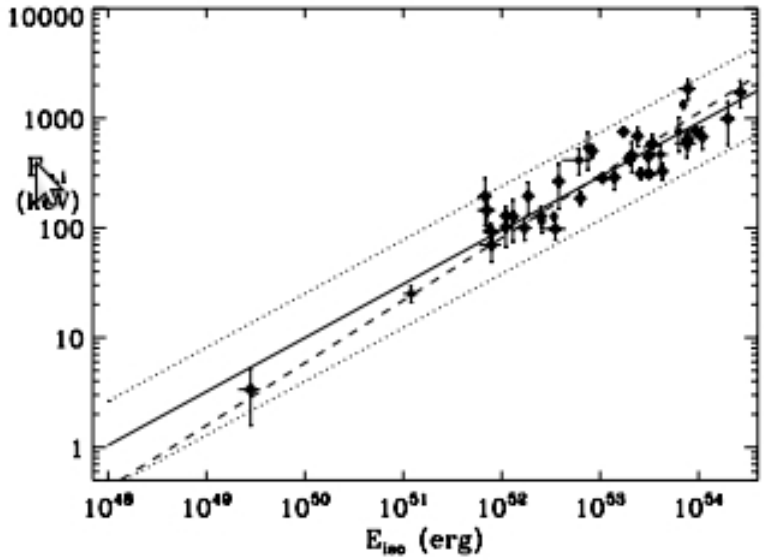

Figure 5.1: Amati relation E_{peak}-E_{iso}. Filled circles corresponds to Swift GRBs. Full line is the best fit, sahded line is the best fit for data without accounting for the sample variance. Dotted line is the logarithmic deviation.[2]

famous and most important one is the so called 'Amati relation', E_{peak}-E_{iso}. It can be written as

$$E_{\rm peak} \propto E_{\rm iso}^{1/2}. \tag{5.1}$$

The parameters needed to obtain E_{iso} is redshift, following the expresion

$$E_{\rm iso} = \frac{4\pi D^2}{1+z} \int_{1/(1+z)}^{10^4/(1+z)} EN(E)\, dE \text{ erg}, \tag{5.2}$$

where D is the source luminosity distance[2]. Amati relation was further confirmed by HETE-2 experiment by [53][2] and agrees with the Swift data.

[2]Hubble constant used in Amati relation is $H_0 = 65$km s^{-1}Mpc^{-1}, whereas in Ghirlanda relation, discussed further is $H_0 = 70$km s^{-1}Mpc^{-1}.

5.2.2 Ghirlanda relation

Whereas Amati relation appears to be valid for most GRBs caught by majority of missions, Ghirlanda relation does not appear to be be so unambiguos. Ghirlanda relation [23] links the peak spectral energy and collimation corrected energy. In this relation, it is assumed that the jet opening angle is Θ, thus the collimation energy can be computed as

$$E_\gamma = (1 - \cos\Theta) E_{\rm iso}. \tag{5.3}$$

The best fit for the relation is

$$E_{\rm peak} = 480 \left(\frac{E_{iso}}{4.3 \times 10^{51} {\rm erg}} \right)^{0.7} {\rm keV}. \tag{5.4}$$

Ghirlanda relation encouteres many problems since it appears that the Swift data does not fit [10][24].

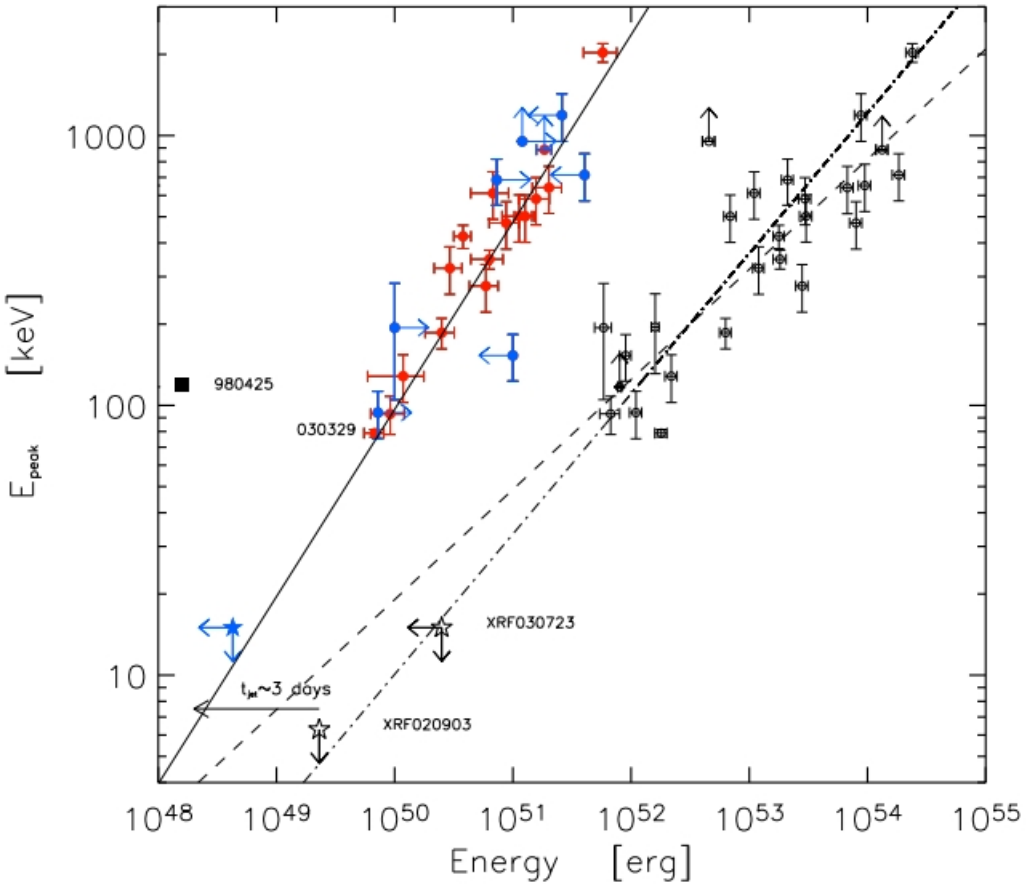

Figure 5.2: Ghirlanda relation is represented by the solid line. Filled symbols are the ones corrected for the collimation angle. The dot dashed line and the grey circles represent the Amati relation [1], while the grey symbols can serve as the lower/upper limits. From [23].

5.3 Another relations?

In general, people have tried to fit multiple relations[25]. The below mentioned suggestion for the correlation is probably the closest one to this work, hence it is quite important. From the independent point of view there may be many more important relations concerning the GRBs. The following text is based on [42].

Natural assumption is that the fainter objects[3] lie in the higher redshifts and apparently this is not necesarilly true for the GRBs.

$$P(z) = \frac{(1+z)^N \tilde{L}(z)}{4\pi d(z)^2}, \tag{5.5}$$

where $P(z)$ is the fluence or flux and $\tilde{L}(z)$ is the emitted isotropic total number of photons/energy. $N \in \{0; 1; 2\}$ depends on the units of the flux. The natural assumption appears to be not necesarilly correct. Apparently the GRBs with small redshifts can be quite fains and vice versa. This can be seen in the graph below.

This result is model-free. It shows that concerning the GRBs, we can expect many surprising results.

[3]Objects with small fluences.

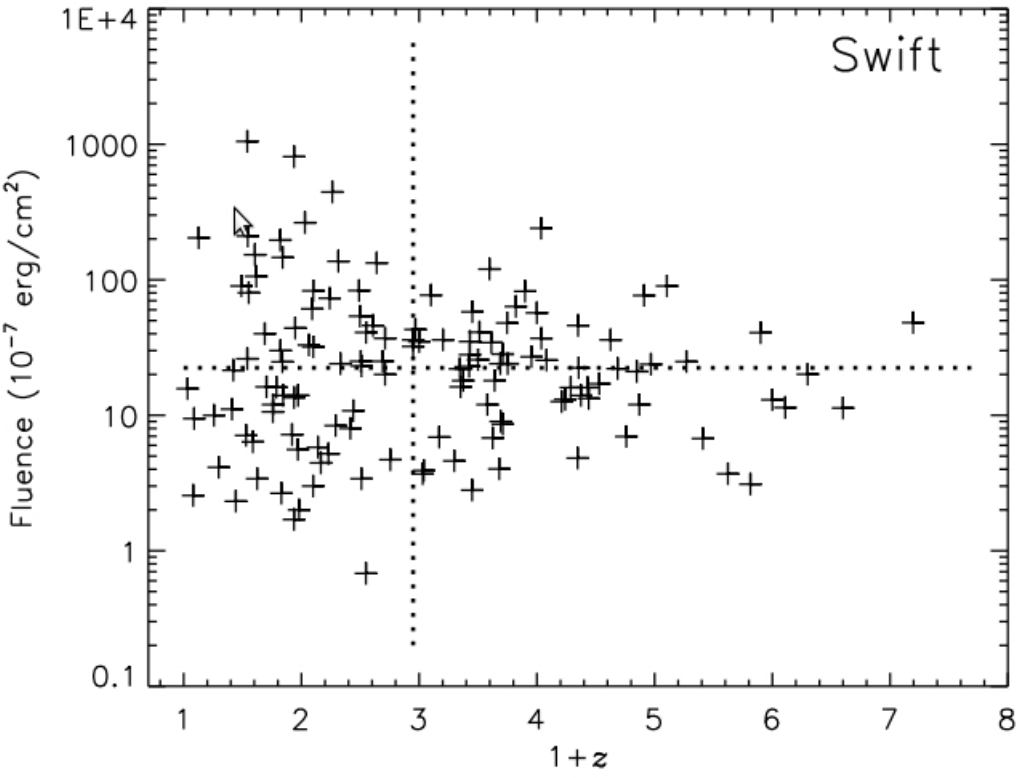

Figure 5.3: Distribution of the fluences of the Swift long GRBs with known redshifts. The dotted lines represents the medians and divide the area into four quadrants. Upper right quadrant represents the objects that are brighter and have higher redshifts. From [42].

6

Gamma-ray bursts progenitors

Since the discovery of the bimodal distribution, it was assumed that different mechanisms are responsible for the short and the long GRBs, although it is assumed that both mechanisms are responsible for a creation of a black hole. There were many models proposed to explain the phenomena, but it is still not quite clear what is responsible for such explosions. The most popular theories for the progenitors of both classes of the GRBs are discussed below.

6.1 Short GRBs

Progenitors of the short GRBs are believed to be merging systems of two black holes (BH - BH), two neutron stars (NS - NS) or combination of these (BH - NS). Those mergers collide, produce a jet near the line of the sight of the ground based observer and the observer detects a flash of gamma-rays. In the ideal case one observes the object before the explosion and thus know the mechanism which led to the event. Unfortunately this approach is not applicable to the case of the short GRBs. Thus we have to rely on the statistical studies of the environment of the GRBs which can lead to some implications about the phenomena.

Studies of the progenitors of the short GRBs are still in nascent phase since the first afterglow was detected in May 2005 (GRB 050509B) [26] and the detection rate is still very small (≈ 10 short GRBs afterglows per year). After the detection of the afterglow, one can try to link the GRB to a galaxy in the same coordinates[1]. This can be done only for some GRBs since some-

[1]The linking for the GRB 050509B was not very clear, it was linked to an elliptical galaxy. The second linked short GBR was GRB050709 which was linked to star-forming dwarf galaxy.

times the GRB can be linked to several galaxies in the field of view.

Short GRBs apparently occur in both types of galaxies - young galaxies with ongoing star-forming activity as well as in ellipticals with the old star population[7]. The short GRBs associated with a starburst galaxies apparently tend to occur in a regions with no star formation (unlike long GRBs). The properties of the host galaxies can be found in [7][47]. Most of the galaxies tend to reside at $z \sim 1$ [6] which is consistent with the redshift distribution of short GRBs. In addition, most of the galaxies that host short GRBs tend to have regular elliptic shapes that can be modeled with Vacoulers profile, are quite large and do not exhibit any signs of merging (at least on a scale more than 10^9 years between the merge and the GRB).

Long GRBs progenitors[2] are believed to originate from one of the most massive stars and they are connected with the supernovae as was first suggested by [15] and confirmed by [21]. It was observed that there is no supernova connection in the short bursts, hence the progenitor of the short GRB is most likely not a massive star [8]. They tend to occur in the old stellar population[3], so it is estimated that they are the product of merging.

Unfortunately the theory is still inconsistent. So no specific models will be discussed here[4].

6.2 Long GRBs

The situation concerning the long GRBs is definitelly better, since the first afterglow was observed in 1997 [51] and the theory is much more developed. Still the progenitors are mostly suggested and not 100% confirmed. The widely accepted model is the 'collapsar model.' The general idea of he model is described in [60]. Collapsars are described as single or binary systems whose core collapses directly to form a black hole. In the next moment after the collaps, the resudial matter quickly accretes onto the black hole and will form a strongly beamed jet. This scenario constricts the progenitors, they should be mostly stripped of the hydrogen and probably also helium shells. It is estimated that the start fitting into the collapsar scenario may be Wolf-

[2]Will be discussed further in the following section

[3]In general, they are usually found on the faint pixels of the image of the galaxy.

[4]The only two competing ones are merging model mentioned in the text and magnetar scenario which is not strongly supported by the observations hence will not be discussed here.

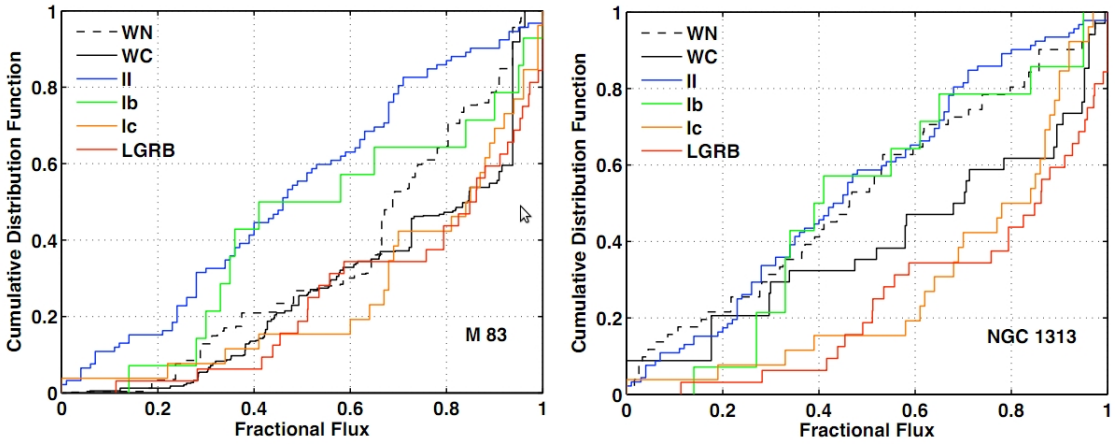

Figure 6.1: Distribution of the two types of the WR stars (WN, WC), types of supernovae and long GRBs in two sample galaxies M83 and NGC 1313 [35], where the detailed studies of the WR stars have been made.

Rayet stars. Those stars are extremely hot and massive (usually more than 30 $M_\odot$) and they tend to lose approximatelly $10^{-5} M_\odot yr^{-1}$. The equatorial rotation speed is quite high, $3000 km \cdot s^{-1}$ [11].

Wolf-Rayet (WR) stars are probably the progenitors of the hydrogen deficit supernovae type Ib/Ic[39]. Thanks to the hydrogen deficit, they would be an ideal progenitor of a 'failed supernovae.' These do not explode , but the result is a prompt formation of a black hole with an accretion disc. This mechanism was first suggested as a possible progenitor of the GRB in [60]. This kind of collapsar is able to produce a jet that is not shorter than ~ 5 s. This agrees quite nicely with the theory. It is assumed, that if the progenitor is such object, GRB should be connected with supernovae [39]. This was later confirmed observationaly, in GRB980425 with supernova SN 1998bw [22], type Ic. Since then, the connection with the supernovae was observed in the most GRBs.

The problem with the WR stars as the progenitors lie in the fact that most of the GRBs lies in the cosmological distances. But the metallicity in the high redshift universe is smaller than in the Solar system. In these conditions the mass loss of the WR stars is smaller and they tend to rotate faster[59][44]. Rotation seems to be a crucial parameter concerning the progenitors, since

the outcome of the GRB should be a Kerr black hole. This rules out the red or blue supergiants. The further restrictions on the progenitors are described in [61].

Another way to find the information about the progenitors is to look at the environment of the host galaxies. The observations show that in most cases, long GRBs tend to occur in a dwarf[5] starburst galaxies [54], moreover in the brightest areas of them. This observational fact supports the theory that the progenitors of the long GRBs are hot and young stars, however in general the statistical sample is still too small.

[5]It is assumed that galaxies used to be smaller, hence the host galaxies of GRBs, located in the cosmological distances, are usually dwarf type.

7
Swift mission

Swift is so far the most succesful mission dedicated to GRBs [66]. Swift was launched on November 20, 2004 on the rocket Delta 7320-10C to a low-Earth orbit as NASA MIDEX project (medium explorers). The satellite was declared fully functional on February 1, 2005. The mission was originally planed to last two years but appeared so succesful that it was extended. At present, there is no plan to end the mission. In the beginning of April, the total number of GRBs was approximately 650. The main scientific goals of the mission were planned as

- Determine the origin of gamma-ray bursts.
- Classify gamma-ray bursts and search for new types.
- Determine how the burst evolves and interacts with the surroundings.
- Use gamma-ray bursts to study the early, high redshifted, universe.
- Perform the first sensitive hard X-ray survey of the sky (secondary objective).

Every year, Swift detects approximately 100 GRBs, which is approximately one third of the estimated number[1], and is able to determine locations within $0.5 - 5$ arcsec. Swift payload consist of three instruments which combined together to work as a multiwavelenght observatory. The instruments are the Burst Alert Telescope (BAT), X-Ray Telescope (XRT) and UltraViolet and Optical Telescope (UVOT).

[1]It is estimated that there is one burst per day.

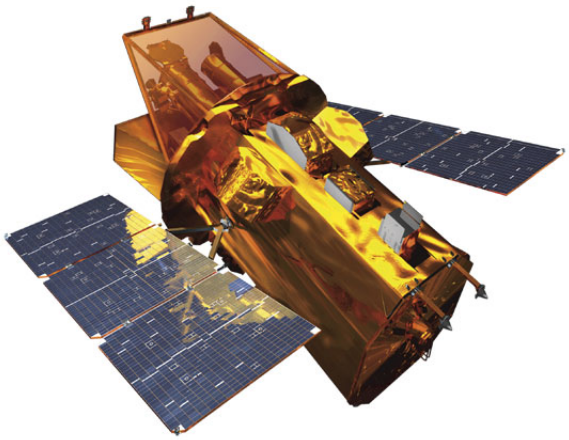

Figure 7.1: Artists impression of the Swift satellite. Courtesy of Los Alamos National Laboratory.

7.1 Burst Alert Telescope – BAT

BAT [68] is a coded aperture mask instrument with sensitivity $15 - 150$ keV. Coded aperture is needed for this kind of the instrument, because gamma rays cannot be easily focused. In general the energy limit for focusing the light with mirrors is approximately 10 keV. The material used for manufacturing the coded aperture mask is lead. Lead can shield gamma rays up to approximately 150 keV, it is mostly transparent to higher energies. The principle of the mask is quite straightforward. The mask consist of $\sim 54,000$ lead tiles in random patter, the detector consists of 32,768 individual CdZnTe elements in the detector plane. Whenever there are incident photons, the lead mask casts a shadow on the detector. Since tha pattern of the mask is random, every direction cast an unique shadow with unique strenght of the signal on the detector. After the shadow is cast, the signal can be decoded. Decoding is done by determining the strength of every possible shifted mask pattern.

Coded aperture has a high sensitivity and large field of view, 1.4 steradians, which can determine the position of the GRB within 4 arcmin in 20 seconds. Energy resolution for the BAT is ~ 7 keV, sensitivity of the detector is $10^{-8}\mathrm{erg} \cdot \mathrm{s}^{-1} \cdot \mathrm{cm}^{-2}$. More technical details are contained in [4].

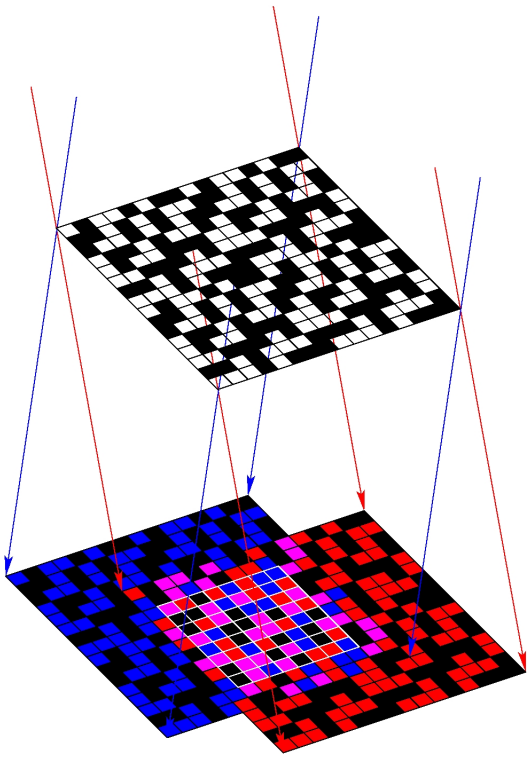

Figure 7.2: Scheme of the coded aperture mask casting different shadows on the detector plane. Courtesy of ISDC.

The BAT monitors the sky continuously, searching for the increase in the rate or image. When an increase is detected, the spacecraft slews to the event position and observes the target in the so called 'burst mode'. Otherwise, when there is no increase, the telescope monitors the hard X-ray sky in the 'survey mode'. In this mode, the instrument collects count-rate data in five-minute time bins for 80 energy intervals.

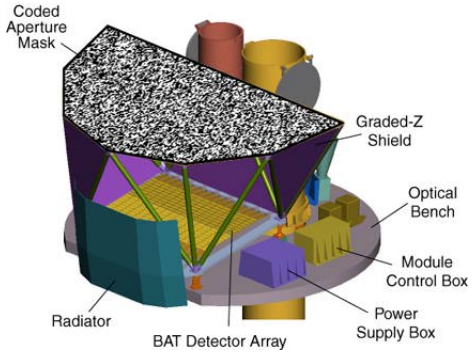

Figure 7.3: Scheme of the BAT detector with coded aperture mask. Courtesy of NASA.

7.2 X-Ray Telescope – XRT

XRT [69] is sensitive in $0.2-10$ keV. It is aligned with the BAT detector, but the field of view is significantly smaller, 23.6×23.6 arcmin and the resolution is 18 arcsec. Since the field of views (FOVs) are aligned, XRT can point to the location of the burst quickly. Usually, XRT will point to the location of the source 20 – 70 s after the discovery. Since the position estimated from XRT is more accurate than from BAT, the coordinates of the burst can be send to the ground based observatories, so the ground based observations can start as ahort as 100 s after the BAT detection.

The XRT uses a Wolter Type I X-ray telescope with 12 nested mirrors, focused onto a single CCD similar to those used by the XMM-Newton EPIC MOS cameras. The CCD consists of an image area with 600×602 pixels (40×40 microns) and a storage region of 600×602 pixels (39×12 microns). The detector is cooled down to approximately 173 K to ensure low dark current. Sensitivity of the detector is $2 \times 10^{-14} \mathrm{erg} \cdot \mathrm{cm}^{-2} \cdot \mathrm{s}^{-1}$ in 10^4 seconds.

The purpose of the XRT is to measure the fluxes, spectra, and light curves of the GRBs and afterglows over a wide dynamic range covering more than seven orders of magnitude in the flux. The observation of the X-ray afterglows is quite important for determining the precise position of the burst which is needed for further studies (i.e. host galaxies). It has a big advantage over

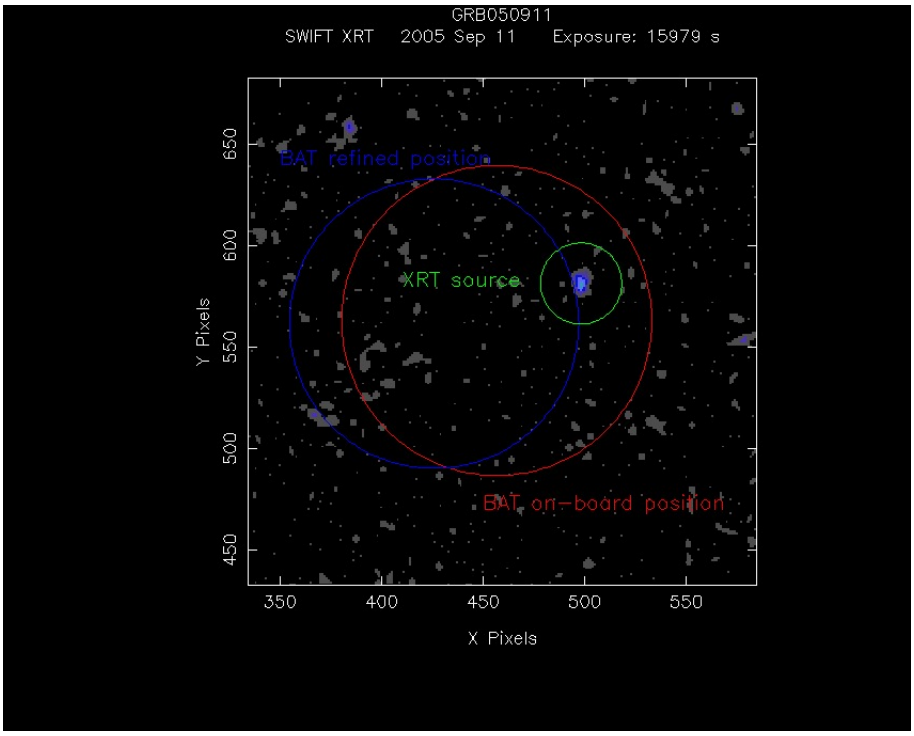

Figure 7.4: Field of view of XRT and BAT and example of refining the positions. Courtesy of NASA.

the ground based observation in the visual band, since only approximately 60% of the GRBs have optical afterglow, while X-ray afterglow is detectable for most bursts.

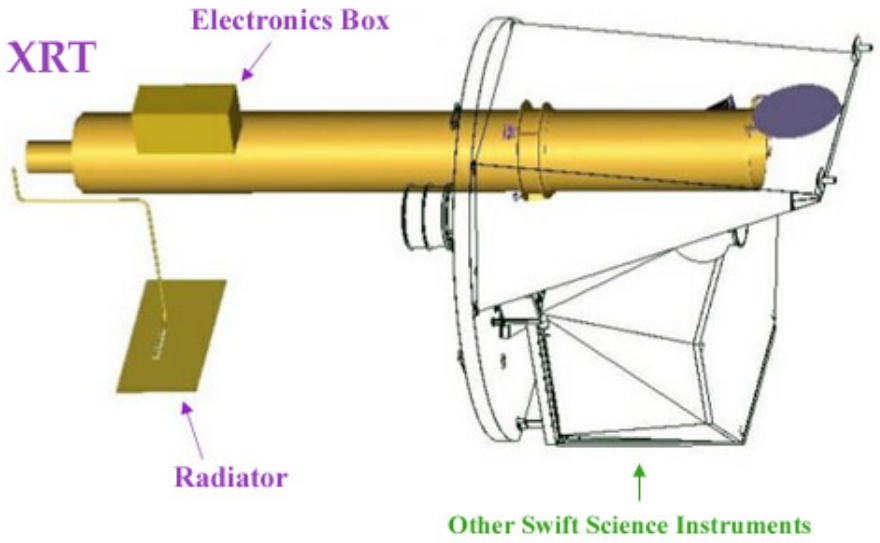

Figure 7.5: Schematic view of XRT. Courtesy of NASA.

7.3 Ultra-Violet and Optical Telescope – UVOT

UVOT [70] is designed for follow up observations of the GRBs. The field of view is 17×17 arcmin and is alligned with BAT and XRT. The telescope can observe optical wavelengts with excess to ultra-violet ($160 - 600$ nm) which is especially important for GRB studies. The telescope itself has 30 cm in diameter and is the design is Ritchey-Chrètinen (Cassegrain telescope with eliminated coma up to third order). The limiting magnitude is 22.3 (1000 s in white light for A0 class star) while the same telescope located on the ground would have a limiting magnitude of ~ 20 due to the presence of the atmosphere and seeing. Stars in the field of view of UVOT are used as an astrometric grid with precision $\sim 0.42''$, usually there are approximately 15 stars in the UVOT field of view that are listed in catalogues. The initial images are immediately send to the ground as a finding chart for ground based observers.

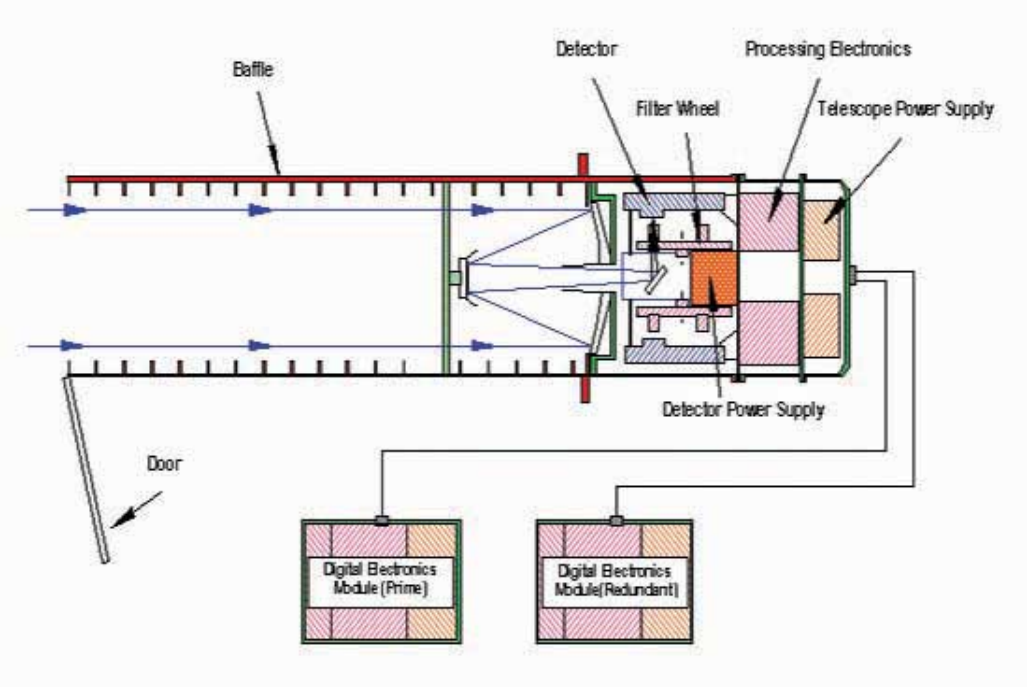

Figure 7.6: A schematics of the UVOT layout, a 30 cm Ritchey-Chrètinen telescope. Courtesy of NASA.

UVOT is equipped with sensitive CCD camera (2048 × 2048 elements) with seven filters - v, b, u, uvw1, uvm2, uvw2 and white filter, which are the same design as was used for XMM-Newton satellite. UVOT has a pre-determined program of exposure times and filter combinations. If the GRB has a redshift between $z \sim 1.3$ and $z \sim 5$, the filtered observations can also measure the photometric redshift of the GRB using the Ly_α cutoff.

In general, the UVOT observations can be described as follows

- 10 s settling exposure.
- 150 s white exposure for the finding chart.
- 50 s UV grism finding chart.

- 250 s u bandfinding chart.
- sets of 20 s exposures for each filter (up to 850s post burst).
- 150 s white finding chart again.
- sets of 20 s exposures in each filter (up to 2700s post burst).
- sets of 200 s exposures in all filters (up to 8400s post burst).
- sets of 900 s exposures in all filters until burst fades.

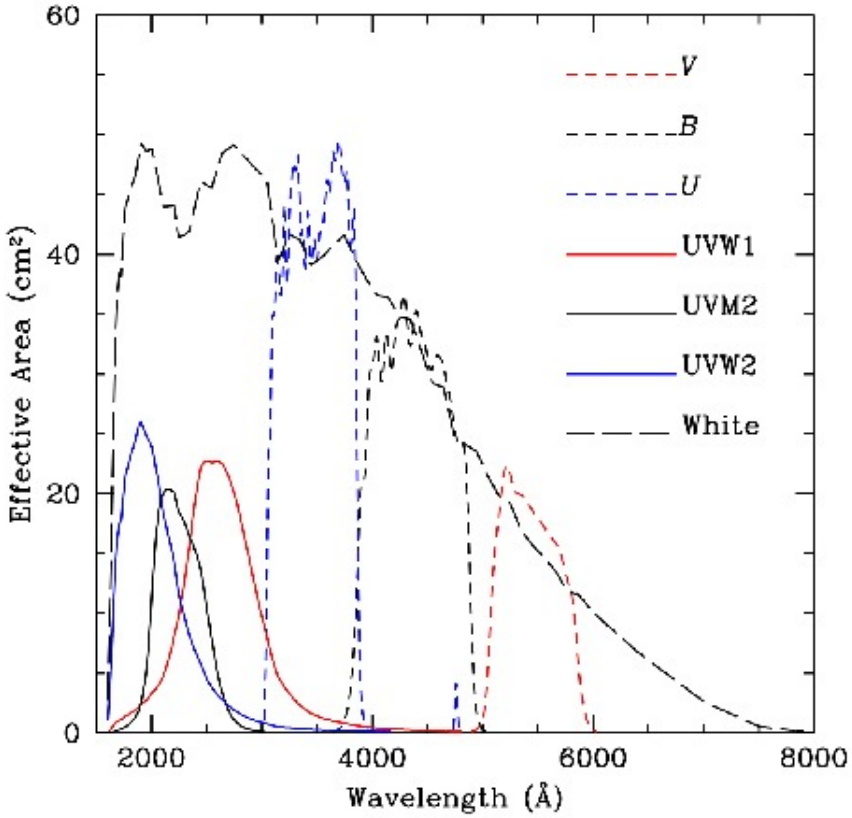

Figure 7.7: Sensitivity of the UVOT filters. Courtesy of NASA.

8

Swift data and the processing

Why Swift?
Swift is orbiting the Earth for more than six years now. It has the biggest number of bursts (more than 650 by the beginning of April) amongst ongoing missions and that makes it an ideal candidate for statistical studies [42]. The other possibility would be to combine data from different ongoing or past missions, but the detectors probably have slightly different sensitivities, thus can bias the data. Another problem concerning other missions is the need for the parameters used in this study (fluence, redshift, optical magnitude and duration). Especially the need to know the redshifts rule out most of the missions since there are only a few bursts with known redshifts from missions excluding Swift. If we look at the sample of BATSE GRBs, only eight have known redshift, Fermi has six bursts with known redshifts[42]. The situation for the RHESSI is even worse since the databases [71] do not contain redshifts at all, hence Swift was chosen for the study. Tables below, from [42], show the known redshifts for the Fermi and CGRO BATSE.

Table 8.1: Table of the CGRO BATSE GRBs with known redshifts. From [42].

GRB	redshift	Fluence[10^{-6} erg $\cdot$ cm^2]
970508	0.835	0.88
971214	3.42	4.96
980425	0.0085	1.67
980703	0.966	14.6
990123	1.600	87.2
990506	1.307	51.6
990510	1.619	8.0
991216	1.02	63.7

Table 8.2: Table of the Fermi GRBs with known redshifts. From [42].

GRB	redshift	Fluence[10^{-6} erg $\cdot$ cm^2]
090323	3.79	1000
090328	0.736	809
090902B	1.822	3740
090926A	2.106	1450
091003	0.897	376
100414A	1.368	1290

Swift data are available online usually within one or two hours after the burst. All the data are accesible via Swift download portal on the address `http://www.swift.ac.uk/swift_portal/` (UK site) with graphic user interface or via ftp, `ftp://heasarc.gsfc.nasa.gov/swift/data/obs` directory, where all the data are stored. The data are analysed using heasoft 6.9, which includes all the tool needed for the Swift analysis.

The files downloaded from the archives usually have names
`sw[Observation ID][Segment Number]b[code].[suffix]`.
`sw` stands for swift and `b` stands for BAT. Segment number is the number of the observation. The first detection has number 000, while i.e. the fourth one will be 004. Observation ID usually starts with 00 and then the trigger number which is specific for every burst. Suffix and the code depend on the routine used. All the data are in `.fits` format, so `.fits` is most common suffix, while the code will usually contain triplet `evt` which stands for event file.

There is a single script called `batgrbproduct` included in heasoft (software used for data analysis in high-energy astrophysics in general) that can be used for analysis of the BAT data. Following sections briefly describe how the script works and what are the products. The whole documentation for the BAT analysis can be found at [3].

The usage is: `batgrbproduct infile= outfile=`

8.1 Mask weighting

In the terms of gamma-rays, the process is also called mask-tagging or ray-tracing. In this procedure the background is subtracted from the image. Since the coded mask depends on the position of the source, one has to know the right ascension and the declination, both in decimal degrees. There are other coordinate systems available for this procedures, i.e. cartesian coordinates and the position of the spacecraft, but those are not commonly used. The procedure which takes care of mask weighting is called `batmaskwtevt`. The procedure does not create a new file, but adds a new column called MASK_WEIGHT into the event file.

The usage is: `batmaskwtevt infile attitude ra dec`

`infile` is an event file from BAT, attitude can be found in the `auxil` directory which is downloaded along with the BAT data for the event.

8.2 Producing the image

An image is build in two steps. Firts one uses the procedure called `batbinevt`. It is used to produce a detector plane image (DPI). The intput data has to be mask weighted. The procedure can be used either for computing weighted light curves and spectra for BAT event and detector plane histogram data (DPH) or for making raw DPIs and histograms.

The usage is: `batbinevt infile outfile outtype timedel timebinalg energybins`

`infile` for our case is the event file (suffix `.evt`), `outfile` will be the DPI (`something.dpi`), `outtype` is the mentioned detector plane image - dpi,

`timedel` is histogram time bin size. In this case the value used is 0, which causes acummulation of the data into a single bin. For this case, there is no maximum bin size (with nonzero value, the maximum bin size is given). `timebinalg` is time binning algorithm, uniform binning (`u` or `uniform`) is used in this case. The last parameter is `energybins`, meaning energy bin list, expressed as a comma-separated list of floating point number ranges. In the case of `batgrbproduct`, there are 4 different energy extensions available: 15-25 keV, 25-50 keV, 50-100 keV and 100-350 keV, or all the information can be stored in one extension covering the whole energy range 15-350 keV.

Next step in producing image from the BAT data is performing a Fast Fourier Transform (FFT) to obtain a sky image. The image is constructed by deconvuling the observed DPI with the BAT mask aperture map. Using this tool, we estimate intentisies and positions of the previously unknown sources.

The usage is: `batfftimage infile outfile attitude`

Where `infile` is the `something.dpi` produced in the previous step and `outfile` is the image, usually with suffix `.img`. Imput for attitude is taken from the auxiliary data in FITS format. If there is no input for attitude, it is not possible to assigne celestial coordinates to the data.

The image of the source is not very exciting, since it is usually a barely visible dot. In most cases, the dot is not even detectable by eyes. For detecting the source, another procedure has to be used - `batcelldetect`. The procedure simply detects the source in the image.

The usage is: `batcelldetect infile outfile snrthresh`

`infile` is the `.img` file produced in the previous step, outfile is an output source list, usually in FITS format which contains new columns, specified in [3]. `snrthresh` stands for pixel signal to noise detection treshold. Value used in batgrbproduct is 6, which means that an excess must be 6 σ above the background level to be considered a detection. The background is measured localy in this procedure.

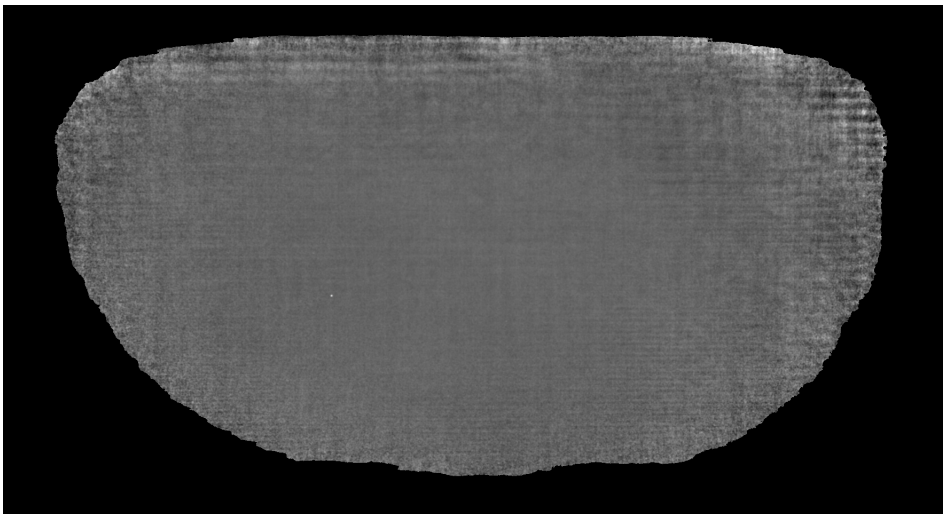

Figure 8.1: The reconstructed image from BAT. Little pale dot, which can be found off center, slightly on the left, is the detected source.

Figure 8.2: Detected source GRB100906A.

8.3 Producing the light curve

First step in producing the light curve is use of the procedure `batbinevt`, which was also used above. The difference between producing the DPI and light-curve is in the type of output, hence the outtype will be `lc`. Time binning algorithm will be `universal` (or `u`) as before, histogram time bin size will be 1.0 which indicated that every bin should have the same size. The only disadvantage is the format of the time in the plotted ligt curve. The plotted time is in the mission elapsed time (MET) which runs from time the mission started (2000). Usually one wants to have time since trigger. This can be done using `ftools`, namely `fcalc` giving TIME-TRIGTIME.

In the next step, the light curve is plotted using `fplot` and the file with suffix `.lc` from the previous step (`batgrbproduct` produces 4 channel with four extensions and 1 channel with one extension light curves so one can choose between them in this step). The usuall convention is to have TIME on the x-axis paremeter and RATE (with errors) on the y-axis. The final product is as follows.

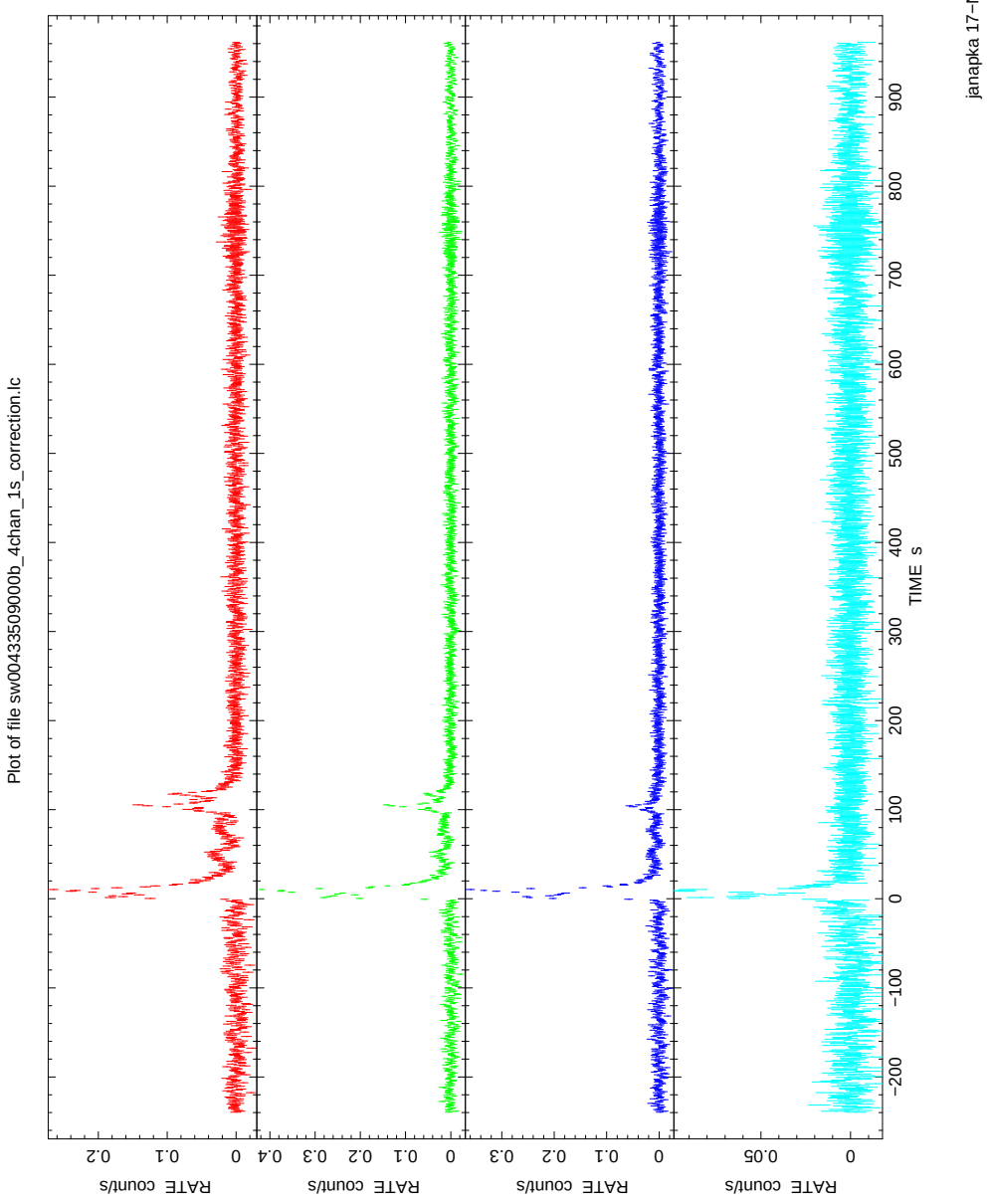

Figure 8.3: Lightcurve of GRB100906A. Channels are 15-25 keV, 25-50 keV, 50-100 keV, 100-350 keV (from the top).

8.4 Determining the timing

The light curve does posses many information, but to estimate the duration of the burst, another procedure has to be used. The procedure is called `battblocks` and is able to estimate interesting time intervals (GTIs) based on the variability of the event or a rare data. The prodecure deals with a single channel light curve which has to have the information about errors.

The usage is: `battblocks infile outfile`

For determining the duration of the burst, we need to add more parameters. In the case of GRBs, the input data will be the ligh curve produced in the previous step and the output file will be with suffix `.gti` which will list the time intervals of a 'constant' flux. Parameter `durfile=dur.gti` will also be needed. The `.gti` file will contain start and stop times in the time since mission started for T_{50}, T_{50}, TXX, 1 second peak flux, the total period covered and the interval used for background subtraction. The procedure also has to be run with `bkgsub=yes` to subtract the background and `countscol=rate` so the procedure looks for RATE column. The `txx` mentioned above alows user to choose another period to determine, i.e. `txx`= 67.0, the durations will be computed for the time in which 67% of all the counts are detected.

8.5 Obtaining the spectra

`batgrbproduct` also computes spectra of the GRBs. These are not used in the work, but since it is a part of the data processing, a short outline of the computation is given below.

Spectra are computed with the procedure `batbinevt` (used in preceeding steps). The `outtype` in this will be pha and the energy binning algorithm and histogram time bin size will be same as for creating the image (`universal` time binning algorithm and 0 histogram time bin size). Energy bin list are taken from the calibration database, so the input for this parameter is CALDB:80. The number 80 means the procedure uses 80 channels which are defined in the calibration database. The spectrum can be also obtained for a specific time interval using `tstart` and `tstop` parameters (in MET). The time interval has to be done manually.

The next step is `batphasyserr` which applies BAT spectral systematic error vector. It estimates the systematic error for every BAT channel. Usually the calibration database (CALDB) is used to estimate these.

The usage is: `batphasyserr infile syserrfile`

Where `syserrfile` will be CALDB and the input will be the `.pha` file which came out of the `batbinevt` procedure. After the systematic error is estimated, the position of the source needs to be ensured (the spacecraft may have slewed and the position could be slightly changed compared to the original position). The procedure used for this step is called `batupdatephakw`. In general, the procedure updates the ray tracing columns in a weighted spectrum. If the procedure is not run, the keywords will reflect the ray-tracing status at the end of the event, which would lead to a wrong response matrix. This procedure requires the auxiliary data from the `batmaskwtevt`.

The usage is: `batupdatephakw infile auxfile`

There the infile is again the `.pha` file that comes out of the `batbinevt`, the `auxfile` can be found in the event data from the BAT, marked as `(obsid)bevtr.fits`.

The last step in creating the spectra is building a response matrix. It is done using `batdrmgen` which computes the full BAT response to incident photons, given the source position information read from the `.pha` file. `batdrmgen` computes the BAT counts spectrum that would be measured of a mono-energetic stream of photons of unit flux with an energy at the bin midpoint were incident on the array. The calculation is repeated for every incident energy bin. The output of the calculation is an $N \times M$ matrix, where N stands for the number of incident photon bins and M is the number of the .pha count bins. Further details about weighting the response matrix are described in [53].

The usage is: `batdrmgen infile outfile hkfile`

Where infile is the `.pha` file, outfile is the response matrix file (usually with suffix `.rsp`). The housekeeping file contains detector bias voltage. The usual parameter here is NONE, which stands for default value 200V.

8.6 Final output

All the output files are stored in the output directory, in subdirectories called lc, pha, dpi, gti, img. In addition there is a text file with the report of the analysis. All the important parameters are stored there. The report looks as follows

```
============================================================
                  BAT GRB EVENT DATA PROCESSING REPORT
    Process Script Ver: batgrbproduct v2.45
    Process Start Time: Mon Nov 15 23:31:28 CET 2010
             Host Name: tatooine
   Current Working Dir: /home/janapka/Documents/Skola/Thesis
/Data/GRB100906A
============================================================

  Trigger: 00433509      Segment: 000

  BAT Trigger Time: 305473773.568   [s; MET]
      Trigger Stop: 305473774.08   [s; MET]
                UTC: 2010-09-06T13:49:27.416480    [includes UTCF
 correction]
       Where From?: TDRSS position message

  BAT
    RA: 28.7092893597252   Dec: 55.6138119348437  [deg; J2000]

     Catalogged Source?: NO
     Point Source?:      YES
     GRB Indicated?:     YES    [ by BAT flight software ]
     Image S/N Ratio:    10.5
     Image Trigger?:     NO
     Rate S/N Ratio:     22.6936114358204  [ if not an image
 trigger ]
     Image S/N Ratio:    10.5

  Analysis Position:   [ source = BAT ]
```

```
    RA: 28.7092893597252   Dec: 55.6138119348437  [deg; J2000]

  Refined Position:   [ source = BAT pre-slew burst ]
    RA: 28.6970955983583   Dec: 55.6336237562119  [deg; J2000]
        { 01h 54m 47.3s , +55d 38' 01.0" }
         +/- 0.544742420042402 [arcmin] (estimated 90% radius
based on SNR)
         +/- 0.186098433524369 [arcmin] (formal 1-sigma fit
error)
    SNR: 72.4416110563395



  Partial Coding Fraction: 0.46875    [ including projection
effects ]

  Duration
     T90: 114.339999914169 +/- 1.59162305818519
        Measured from: 1.73199999332428
                    to: 116.071999907494     [s; relative to
TRIGTIME]
     T50: 55.2559999227524 +/- 8.27925119656045
        Measured from: 7.40799999237061
                    to: 62.663999915123     [s; relative to
TRIGTIME]



  Fluence
     Peak Flux  (peak 1 second)
        Measured from: 10.4799999594688
                    to: 11.4799999594688     [s; relative to
TRIGTIME]
     Total Fluence
        Measured from: -0.192000031471252
                    to: 130.455999970436     [s; relative to
TRIGTIME]
```

```
              Band 1      Band 2      Band 3      Band 4
               15-25       25-50       50-100     100-350      keV
 Total      6.315714    7.099001    4.819537    0.988226
            0.075655    0.078152    0.069704    0.053890 [error]
 Peak       0.268627    0.421543    0.366485    0.090333
            0.012534    0.014276    0.013897    0.009308 [error]

     [ fluence units of on-axis counts / fully illuminated
detector ]

============================================================
```

To plot the lightcurve, one needs the files stored in lc directory. As was mentioned, the product of the batgrbproduct script produces several lightcurves - 1 channel (all energies between 15 and 350 keV), 4 channels (four energy bands, 15-25 keV, 25-50 keV, 50-100 keV, 100-350 keV) and bayesian blocks. All of them can be plotted in several time binnings - 4 ms, 64 ms, 1 s, etc. The one used for ploting the light curves used in this work is 4 channel with one 1 s binning.

9

Morphology of gamma ray bursts revisited

The analysis was performed on the franction of the Swift GRBs. The first restriction was known redshift. The total number of bursts with known redshift is 182 (in the middle of April 2011). However not all the bursts have all the data available, usual problem was missing telemetry data which are needed for the `batgrbproduct` procedure. Some of the data were also damaged so the `batgrbproduct` didn't produce an output. The outputs can also be checked at `http://swift.gsfc.nasa.gov/docs/swift/archive/grb_table/`. Some of the GRBs don't have the lightcurve available, so these were also ruled out. The final sample is 137 GRBs, both long and short.

All the lightcurves were sorted according to the appearance of the lightcurve. The main criteria for the sorting were following

- Single/double peak.
- Spikiness of the peak.

Using this criteria, the sample of the 140 GRBs was divided into four newly proposed groups. There are only three GRBs that don't fit into the sorting. These three have three peaks separated by a quiet phase and since there are only three of them, they won't be considered as a group. The sorting is not done automaticaly but by eye. It is known that there is no function that can fit the light curves and in general, all the GRBs are believed to have original imprint. The sorting presented here looks only for the common features, so there is no diference between double peaked GRB which have the first peak lower and the second peak higher and the GRB with the first

peak higher and the second peak lower. The complete catalogue of the light curves is on the attached CD.
The four proposed groups are as follows:

- Double peaked structure.
- Single peaked structure.
- Complex peak.
- Flat 'lazy' peak.

9.1 Double peaked GRBs

These GRBs have two spiky peaks, usually (but not by a rule) separeted by a quiet phase. The peaks appear to be quite simple and not very broad. Total number of the double peaked GRBs is 27. Usual light curve and the table of these GRBs are on the following pages.

The peak reflects emission of the baryonic matter, so it can be estimated, that the matter was ejected in the two phases. Another possibility would be a complicated shock wave, as is explained by the internal shock scenario [48][50].

Table 9.1: Overview of the double peaked GRBs from Swift.

GRB	T_{90} [s]	Fluence[10^{-7} erg $\cdot$ cm^2]	UVOT mag	redshift
100704A	197.5	60	20.0	3.6
100704A	63.6	210	19.49	0.542
100704A	37	4.7	19.76	1.755
100704A	34.6	37	16.40	1.71
090715B	266	57	21.0	3.00
090424	48	210	16.86	0.544
081203A	294	77	13.30	2.1
081203A	185.5	43	15.64	1.9685
081203A	280	25	18.03	1.692
080916A	60	40	17.55	0.689
080707	27.1	5.2	19.97	1.23
080603B	60	24	16.48	2.69
080413A	46	35	15.08	2.433
080411	56	264	18.05	1.03
070411	121.5	27	17.40	2.954
061121	81.3	137	17.06	1.314
060926	8	2.19	19.0	3.208
060729	115.3	26.1	17.30	0.54
060714	115	28.3	18.6	2.71
060607A	102.2	25.5	15.35	3.082
060526	298.2	12.6	17.2	3.21
060418	103.1	83.3	14.99	1.489
060115	139.6	17.1	19.5	3.53
051221A	1.4	11.5	19.2	0.547
050820A	26	34.4	18.2	2.6147
050319	152.5	13.1	17.5	3.24
050318	32	10.8	19.7	1.44

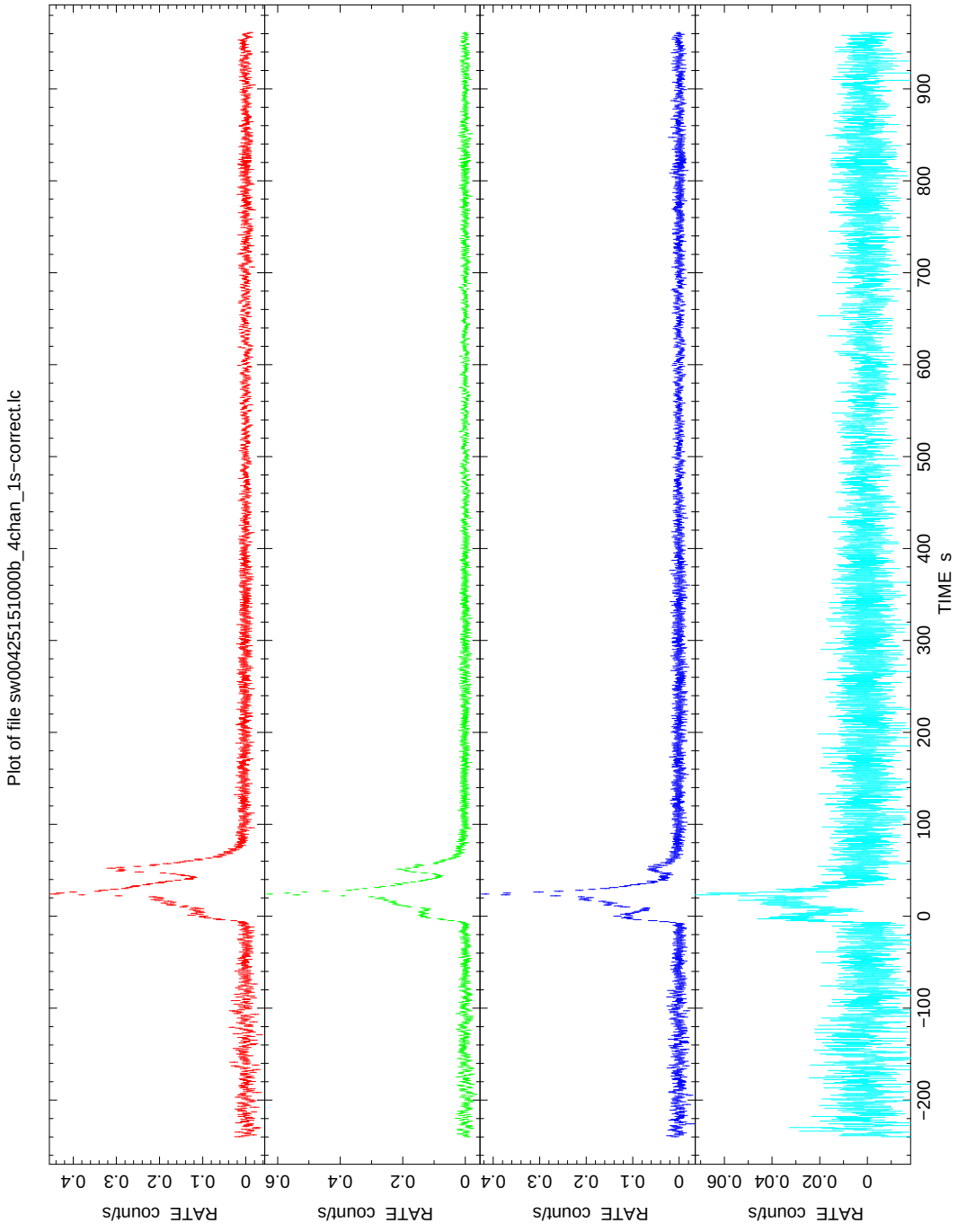

Figure 9.1: Example of a double peaked GRB100621A.

9.2 Single peaked GRBs

These GRBs have one peak, usually quite spiky. The peak can be complex or just one spike. Total number of single peaked GRBs in the sample is 51. Usual light curve and the table of these GRBs are on the following pages.

This light curve exhibit simple behavior so we can assume that the event was quite simple in its nature. The baryonic matter was apparently ejected only once or the physics of the shock is quite simple [48][50].

Table 9.2: Overview of the single peaked GRBs from Swift.

GRB	T_{90} [s]	Fluence[10^{-7} erg $\cdot$ cm^2]	UVOT mag	redshift
110213A	48	59	16.19	1.46
110128A	30.7	7.2	20.09	2.339
100816A	2.9	20	21.56	0.8034
100724A	1.4	1.6	18.31	1.288
100316B	3.8	2	18.28	1.180
091127	7.1	90	17.0	0.49034
091018	4.4	14	16.4	0.971
090926B	109.7	73	19.19	1.24
090510	0.3	3.4	18.46	0.903
090426	1.2	1.8	19.04	2.609
090205	8.8	1.9	20.7	4.6497
090102	27	0.68	17.02	1.547
081222	24	48	16.20	2.77
081007	10	7.1	17.5	0.5295
080913	8	5.6	20.08	6.44
080805	78	25	19.81	1.505
080804	34	36	17.17	2.2045
080721	16.2	120	14.98	2.602
080605	20	133	18.53	1.6398
080516	5.8	2.6	21.1	3.2
080430	16.2	12	17.64	0.767
080413B	8	32	17.64	1.10
080330	61	3.4	18.9	1.51
080210	45	18	17.6	2.641
071117	6.6	24	21.2	1.331

Table 9.3: Overview of the single peaked GRBs from Swift.

GRB	T_{90} [s]	Fluence[10^{-7} erg $\cdot$ cm^2]	UVOT mag	redshift
071031	180	9	19.08	2.692
070810A	11	6.9	17.1	2.17
070724A	0.4	0.3	19.5	0.457
070714B	64	7.2	20.36	0.92
070508	20.9	196	19.7	0.82
061222B	40	22.4	19.77	3.355
061201	0.76	3.34	20.8	0.111
061110B	134	13.3	20.14	3.44
061110A	40.7	10.6	20.42	0.758
060908	19.3	28	16.85	2.43
060904B	171.5	16.2	18.64	0.703
060707	66.2	16	19.65	3.43
060502A	28.4	23.1	18.70	1.51
060223A	11.3	6.73	17.7	4.41
060210	255	76.6	20.1	3.91
060206	7.6	8.31	18.8	4.048
060108	14.3	3.69	19.4	2.03
051111	46.1	40.8	19.33	1.549
051109B	14.3	2.56	20.8	0.080
051016B	4	1.7	20.5	0.9364
050908	19.4	4.83	19.3	3.3437
050802	19	20	17.07	1.71
050724	96	9.98	18.84	0.257
050603	12.4	63.6	18.2	2.821
050525A	8.8	153	14.97	0.606
050505	58.9	24.9	19.82	4.27

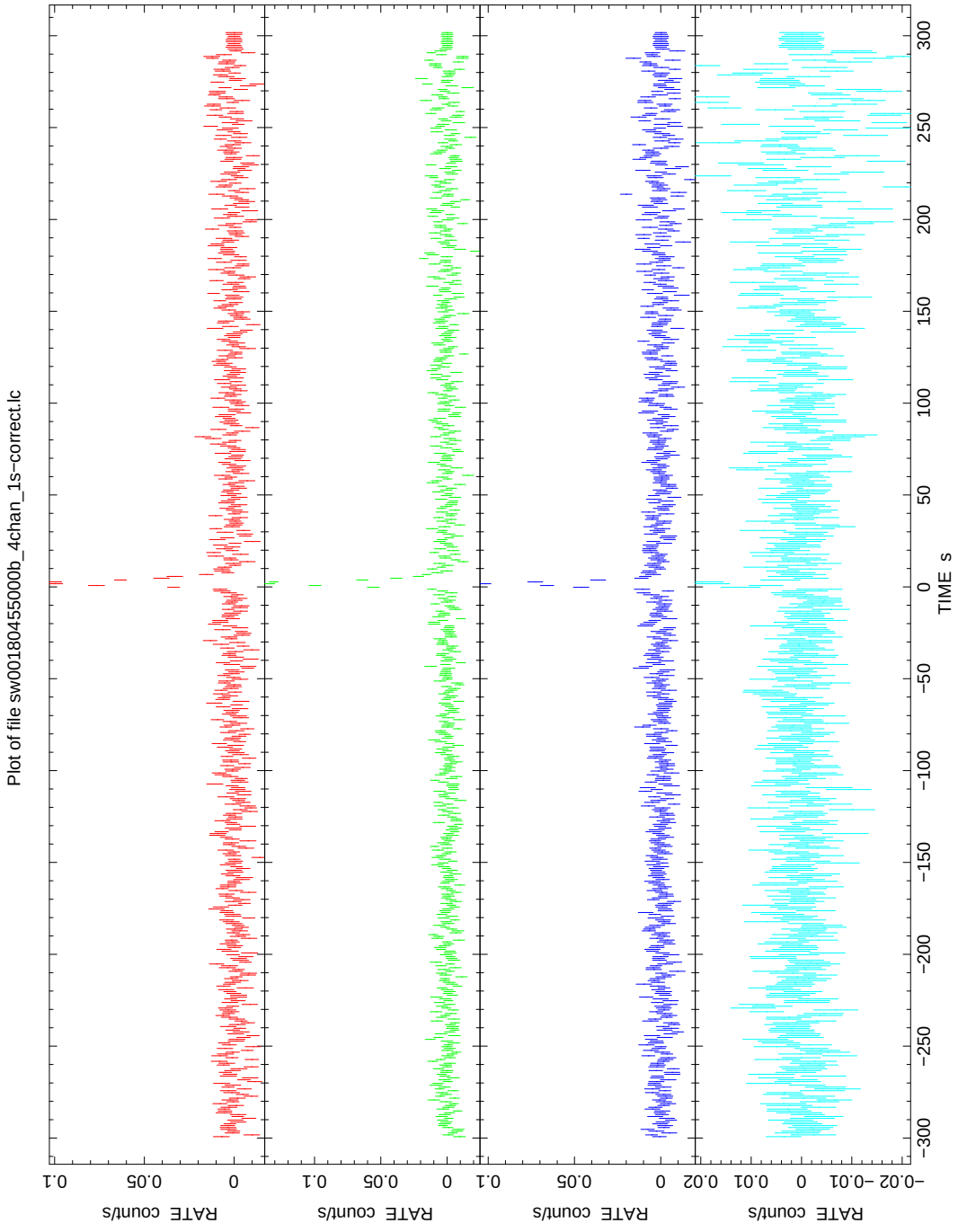

Figure 9.2: Example of a single peaked GRB060206.

9.3 'Lazy' peaked GRBs

These GRBs can be characterized with a light curve which is not very spiky. The lightcurve resembles a simple hill with no other features. Total number of the 'lazy' GRBs is 35. Usual light curve and the table of these GRBs are on the following pages.

The 'lazy' peaked GRBs are of the same nature as the groups mentioned before, but we can assume that the jet is slightly off the line of the sight hence the light curve is not very spiky. The other explanation for this 'lazy' peak may be the domination of the external shock which is believed to produce smooth light curves [48][50].

Table 9.4: Overview of the lazy peaked GRBs from Swift.

GRB	T_{90} [s]	Fluence[10^{-7} erg $\cdot$ cm^2]	UVOT mag	redshift
101219B	34	21	17.55	0.5519
100901A	439	21	18.50	1.408
100418A	7	3.4	19.90	0.6235
100302A	17.9	3.1	18.82	4.813
100219A	18.8	3.7	19.7	4.6667
091109A	48	16	19.94	3.076
090726	67	8.6	19.98	2.71
090519	64	12	19.8	3.85
090313	79	14	20.10	3.375
081118	67	12	19.79	2.58
081029	270	21	18.66	3.8479
080906	147	35	18.61	2.0
080710	120	14	17.06	0.845
080604	82	8	20.1	1.416
080520	2.8	0.55	19.96	1.545
071122	68.7	5.8	21.2	1.14

Table 9.5: Overview of the lazy peaked GRBs from Swift.

GRB	T_{90} [s]	Fluence[10^{-7} erg $\cdot$ cm^2]	UVOT mag	redshift
070802	16.4	2.8	19.96	2.45
070506	4.3	2.1	19.1	2.31
070419A	115.6	5.58	20.0	0.97
070110	88.4	16.2	20.3	2.352
061217	0.21	0.42	20.3	0.827
060906	43.5	22.1	20.1	3.685
060605	79.1	6.97	16.53	3.78
060604	95	4.02	21.2	2.68
060602A	75	16.1	21.3	0.787
060522	71.1	11.4	20.1	5.11
060512	8.5	2.32	15.88	0.4428
060502B	0.131	0.4	20.29	0.287
060116	105.9	24.1	19.2	6.6
050826	35.5	4.13	19.4	0.297
050824	22.6	2.66	20.02	0.83
050814	150.9	20.1	20.5	5.3
050813	0.45	0.44	19.1	1.8
050730	156.5	23.8	17.842	3.96855
050509B	0.073	0.09	21.1	0.225

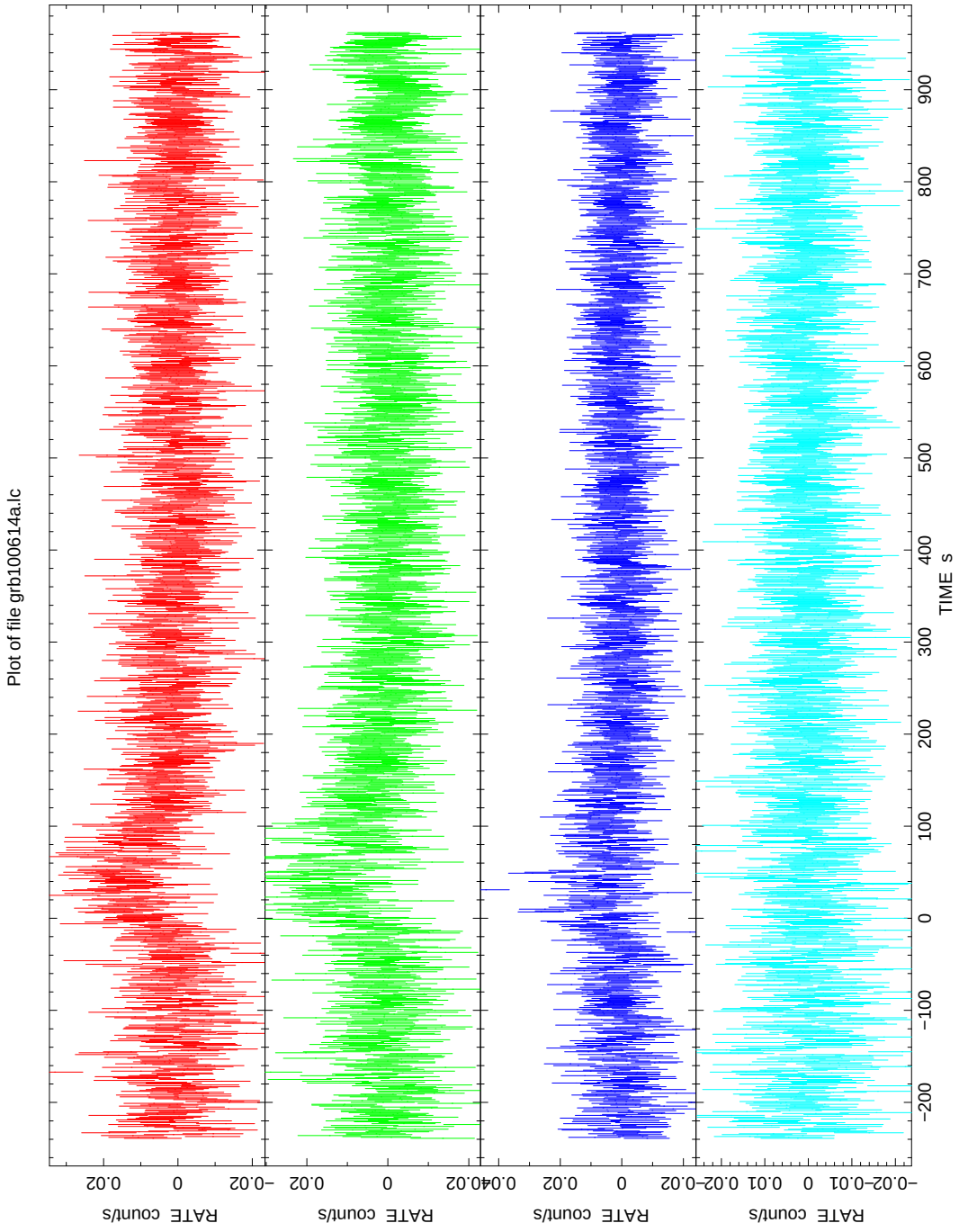

Figure 9.3: Example of a lazy peaked GRB100614A.

9.4 Complex peaked GRBs

These GRBs have complex lightcurves that consist of one hilly peak with a lot of spikes. There is no quiet phase between the spikes, there is always some signal between the minor spikes. In general, there are more than two peaks detected in the first two extensions (15 - 25 keV and 25 - 50 keV). Total number of complex peaked GRBs is 21. Usual lightcurve and the table of the complex peaked GRBs are on the following pages. The definition of this group is the most ambivalent. The complex structure may be caused just by the fact, that there was high S/N ratio, so the minor geometrical features were detectable, unlike in the previous groups.

The complex structure may also correspond to the complicated nature of the medium surrounding the progenitor of complicated shock waves [48][50].

Table 9.6: Overview of the complex peaked GRBs from Swift.

GRB	T_{90} [s]	Fluence[10^{-7} erg $\cdot$ cm^2]	UVOT mag	redshift
110205A	257	170	15.76	2.22
101219A	0.6	4.6	19.7	0.718
100814A	174.5	90	17.91	1.44
100413A	191	62	20.4	3.9
091029	39.2	24	17.81	2.752
090927	2.2	2	19.0	1.37
090812	66.7	58	18.17	2.452
090618	113.2	1050	15.60	0.54
090423	10.3	5.9	19.6	8.0
090418A	56	46	17.31	1.608
081121	14	41	17.58	2.512
080810	106	46	14.06	3.35
080607	79	240	19.44	3.036
080319C	34	36	18.09	1.95
080310	365	23	17.38	2.4266
071227	1.8	2.2	20.46	0.383
070529	109.2	25.7	17.1	2.4996
070521	37.9	80.1	20.4	0.553
070429B	0.47	0.63	19.3	0.904
061007	75.3	444	12.84	1.261
060510B	275.2	40.7	21.2	4.9

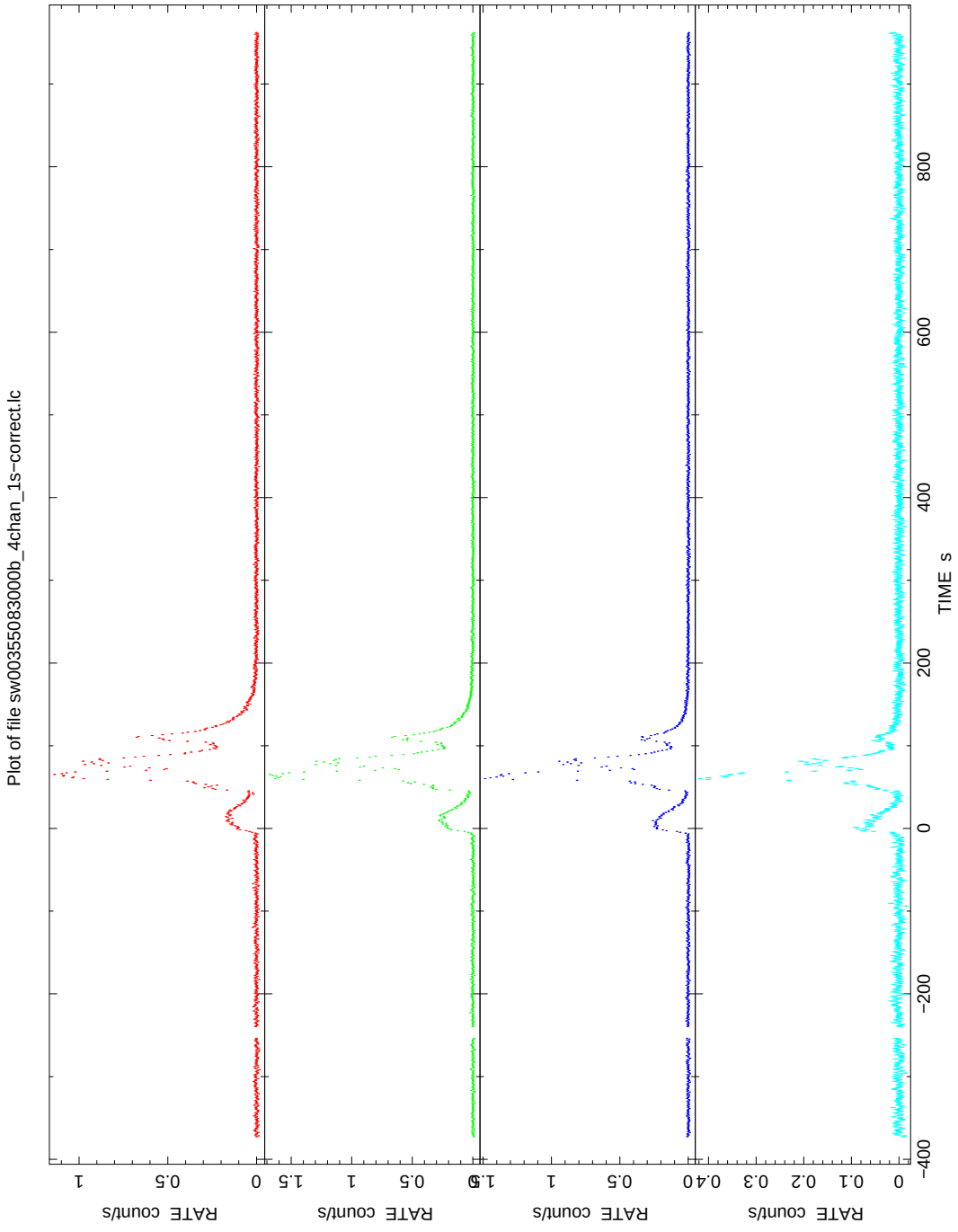

Figure 9.4: Example of a complex peaked GRB090618.

10 Possible correlations

Possible correlations within the groups mentioned in the previous chapter are discussed here. There are four parameters available for every burst - redshift, visual magnitude in V filter from UVOT, duration (in terms of T_{90}) and the fluence (10^{-7} erg $\cdot$ cm^2) determined. All the expected correlations and observed correlations are discussed in the conclusions.

10.1 Correlations within the double peaked group

We estimated that there may be some correlation between the opticaly bright and double peaked GRBs since this trend appeared in the opticaly bright bursts from the RHESSI database [71]. Unfortunately this hypothesis was not confirmed by the available Swift data. The group of the double peaked GRBs is the most homogenous one, since all the parameters seem to be equally distributed. Though we can see an interesting fact proposed by [42] in figure 10.5. The fluence seem to be independent on the redshift.

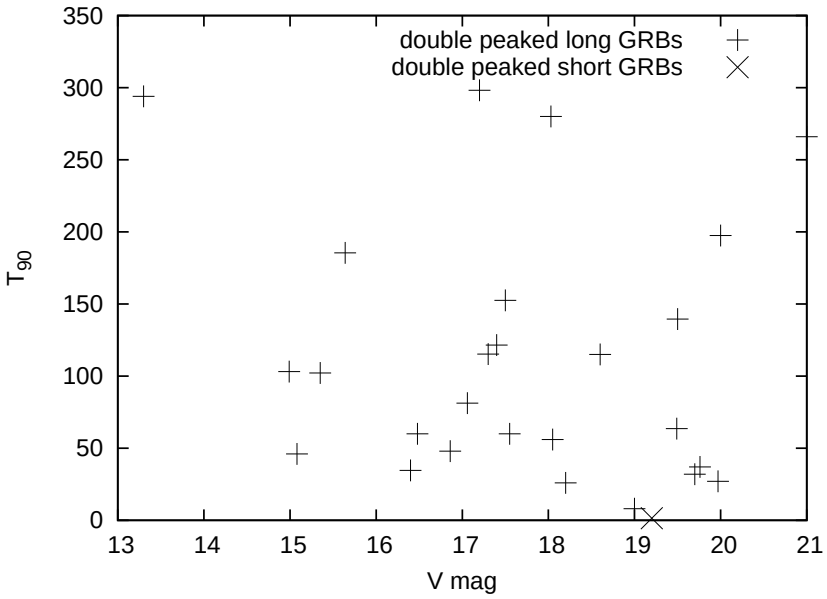

Figure 10.1: Double peaked gamma ray burst in the duration - UVOT magnitude relation.

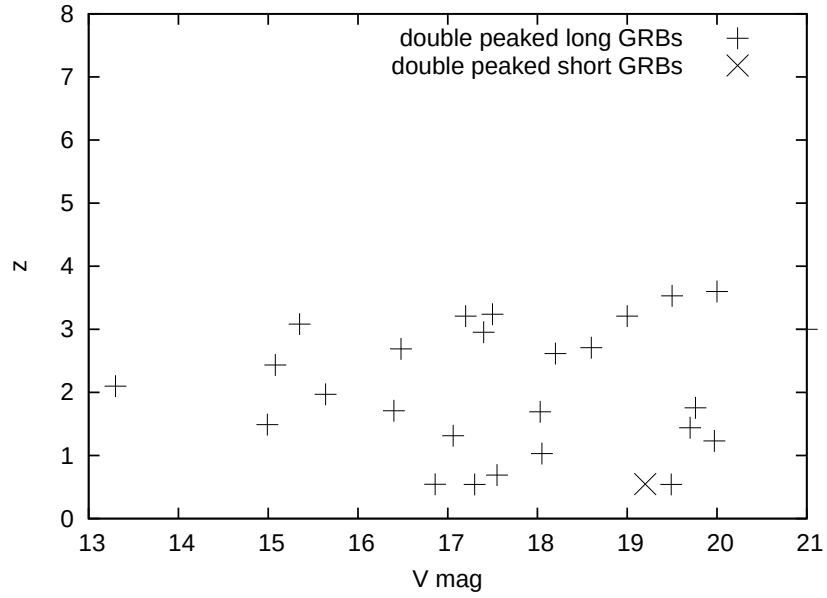

Figure 10.2: Double peaked gamma ray burst in the redshift - UVOT magnitude relation.

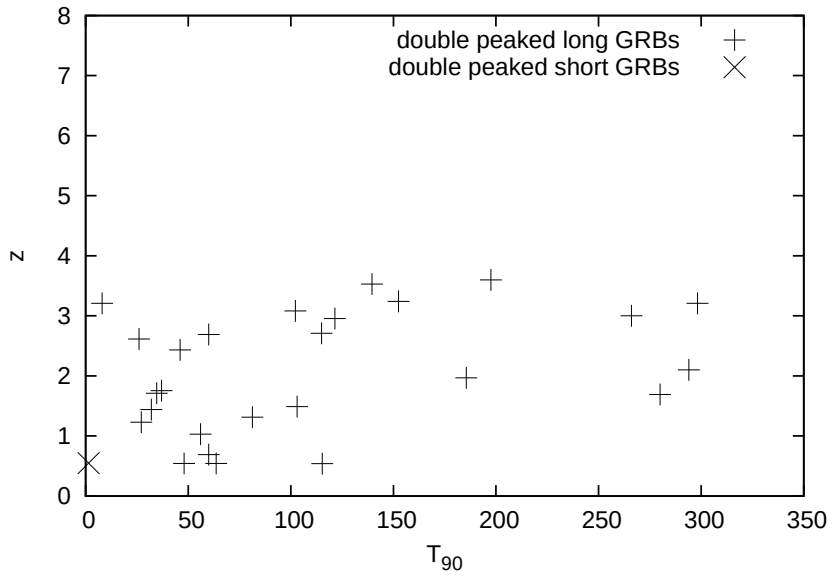

Figure 10.3: Double peaked gamma ray burst in the redshift - duration relation.

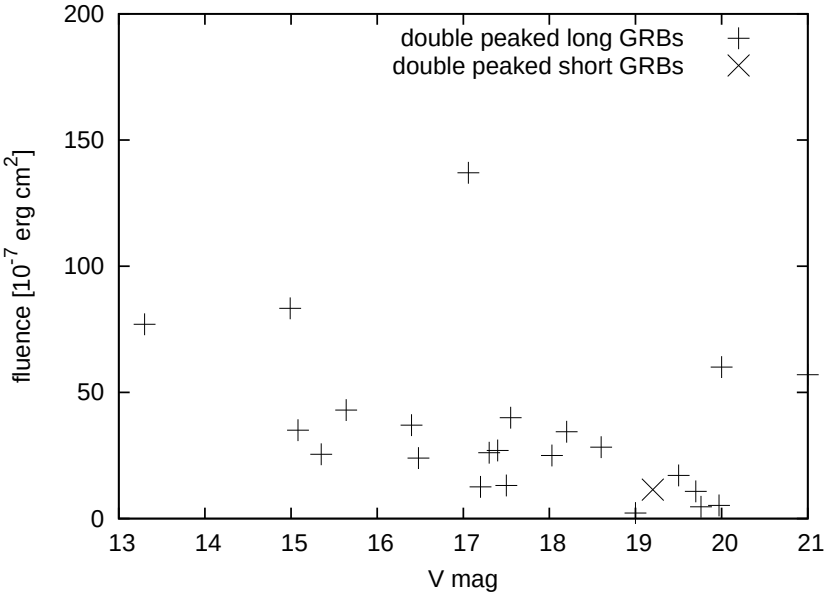

Figure 10.4: Double peaked gamma ray burst in the total fluence - UVOT magnitude relation.

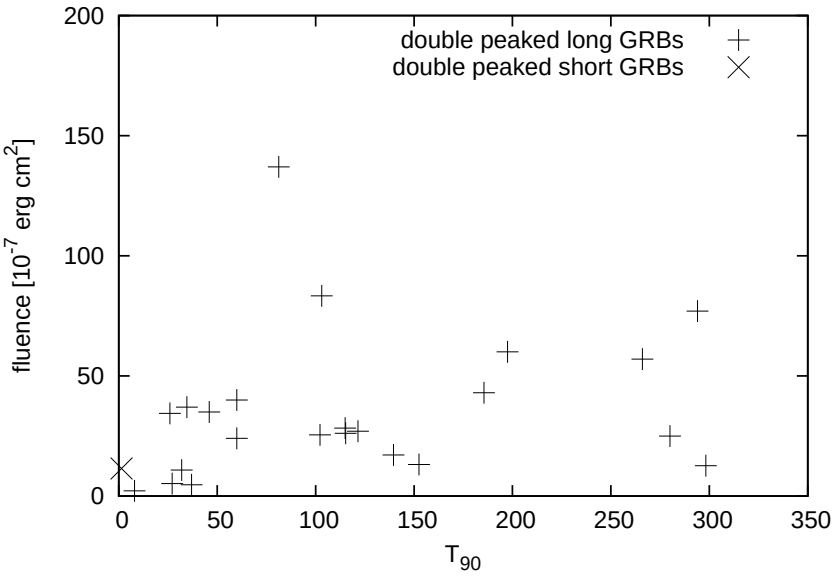

Figure 10.5: Double peaked gamma ray burst in the total fluence - duration relation.

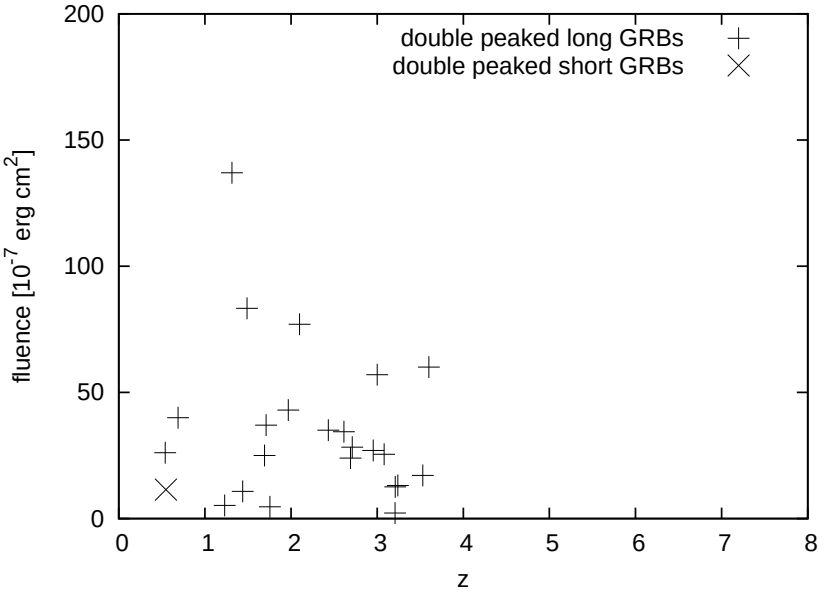

Figure 10.6: Double peaked gamma ray burst in the total fluence - redshift relation.

10.2 Correlations within the single peaked group

The single peaked group holds the biggest number of the bursts (51). They appear to be equally distributed within all magnitudes and quite naturally, they tend to be shorter than the other events. The only exceptions are the bursts GRB060210 ($T_{90} = 255$ s), GRB060904B ($T_{90} = 171.5$ s), GRB071031 ($T_{90} = 180$ s) and GRB061110B ($T_{90} = 134$ s). In the first three mentioned samples, the GRBs have sharp spike located not close to the trigger time, so it can be estimated, there may be some precursors and probably some extended emission without recognizable geometry thanks to low S/N ratio. The last case appear to have one broad peak lasting for a long period. It is highly possible that with more sensitive detector and hence clearer view on the morphology of the lightcurve, those GRBs would not be classified as a single peaked. In the end, we can exclude them from the plot. Considering this constraint, it can be seen that the single peaked GRBs tend to be quite short.

Concerning the other two graphs, single peaked GRBs tend to be equally distributed in all the measured reshifts. Concerning the duration and the redshift correlation in figure 10.2, there is a noticeable clumping at $z \sim 1$ which agrees with [6].

In the terms of fluence and hence cosmological parameters mentioned in [42] we see the distribution does not follow any rule.

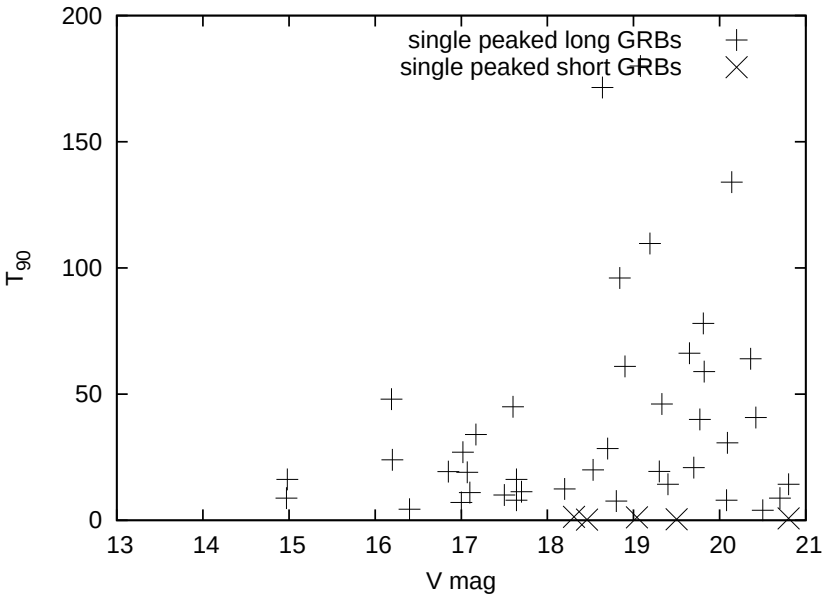

Figure 10.7: Single peaked gamma ray burst in the duration - UVOT magnitude relation.

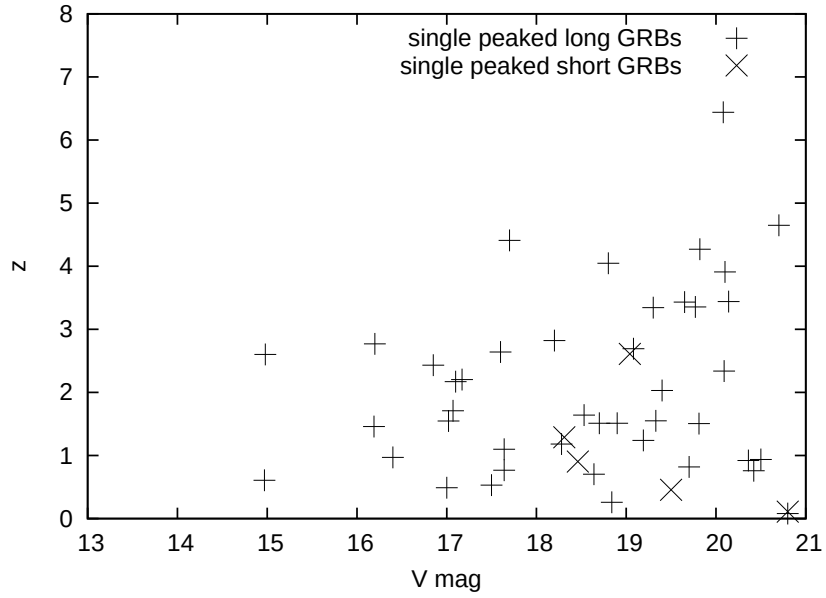

Figure 10.8: Single peaked gamma ray burst in the redshift - UVOT magnitude relation.

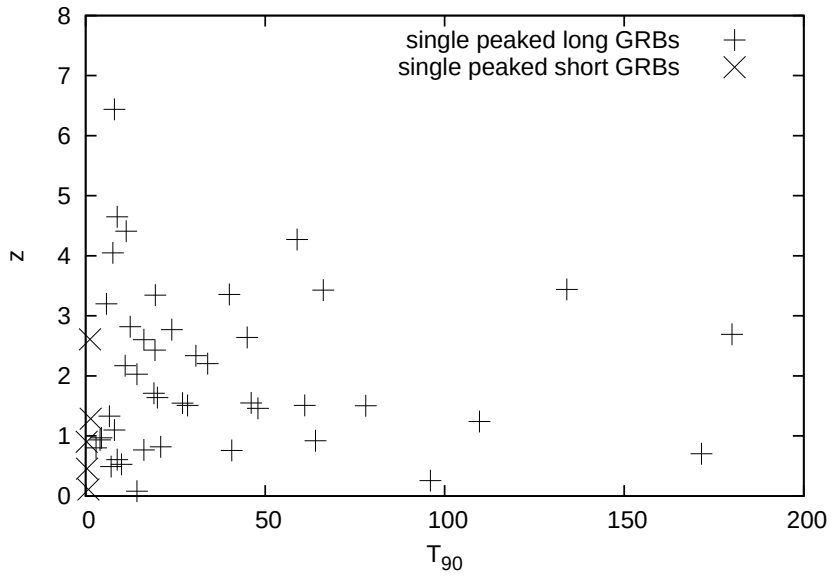

Figure 10.9: Single peaked gamma ray burst in the redshift - duration relation.

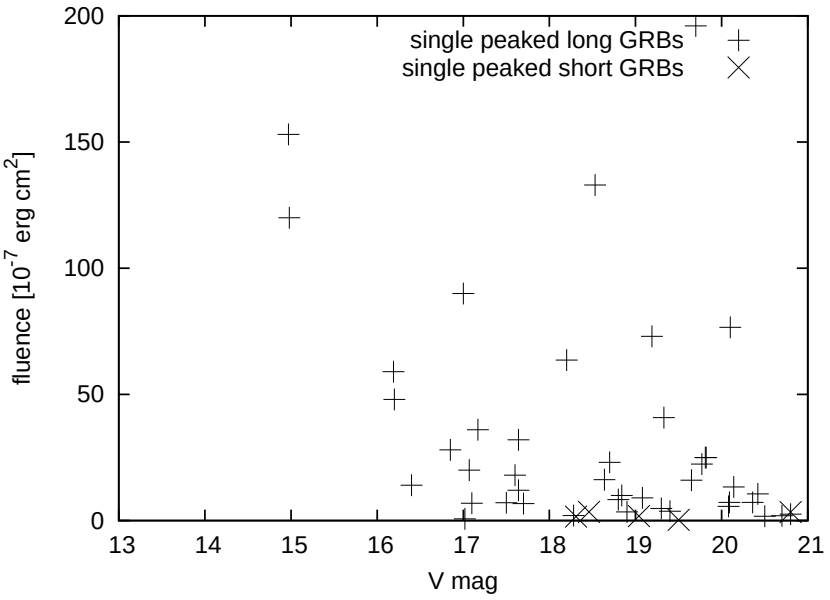

Figure 10.10: Single peaked gamma ray burst in the total fluence - UVOT magnitude relation.

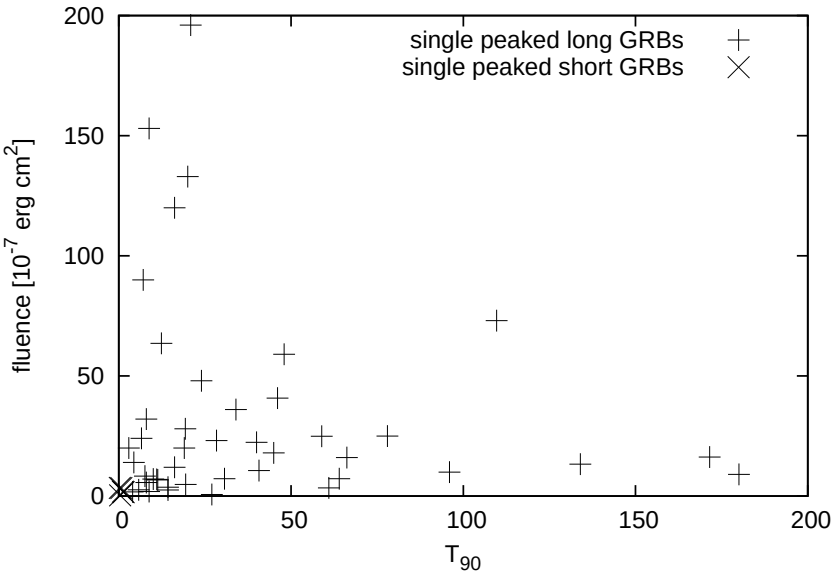

Figure 10.11: Single peaked gamma ray burst in the total fluence - duration relation.

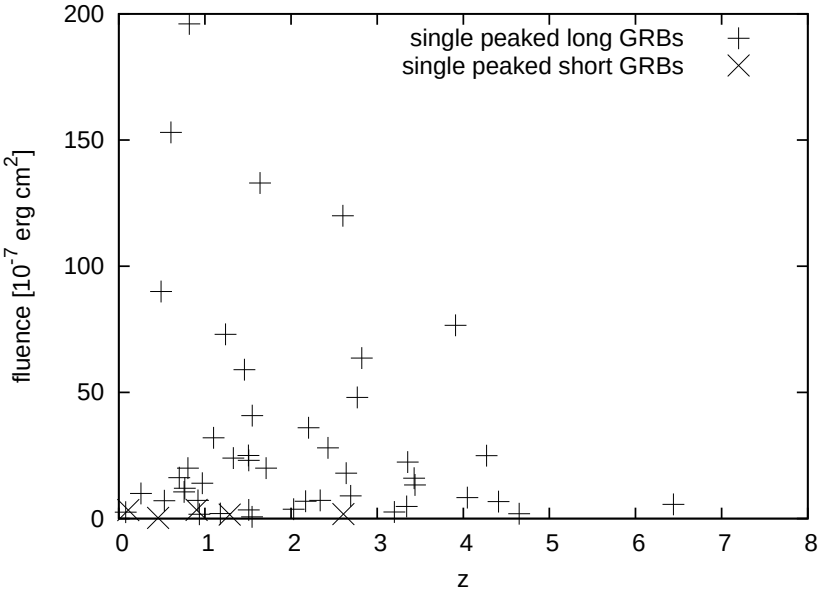

Figure 10.12: Single peaked gamma ray burst in the total fluence - redshift relation.

10.3 Correlations within the 'lazy' peaked group

This group exhibits probably one of the most interesting correlations. Concerning the time, the 'lazy' peaked GRBs tends to be equally distributed. This is quite surprising since one would expect this group to have longer durations in general. The most interesting clumping is noticeable in the graphs showing UVOT magnitude in V filter, graphs 10.3 and 10.13. It is clearly visible, that the 'lazy' peaked GRBs tend to cluster around UVOT $\mathrm{mag_V} = 20$. This is apparently not related to the redshift, since it is clearly visible in the second graph, 10.13, that the distribution in the terms of redshift is quite homogenous, as well as in fluences as can be seen in graph 10.15.

It can be also seen in 10.3 that the time and the redshift are completely unrelated, since the 'lazy' peaked GRBs tend to be equally distributed. The fluences for this group seem to be low in general.

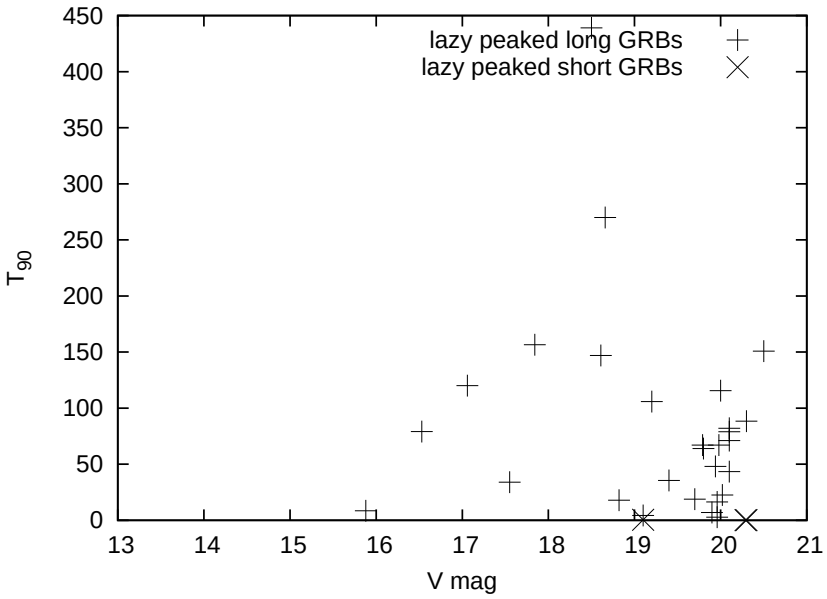

Figure 10.13: Lazy peaked gamma ray burst in the duration - UVOT magnitude relation.

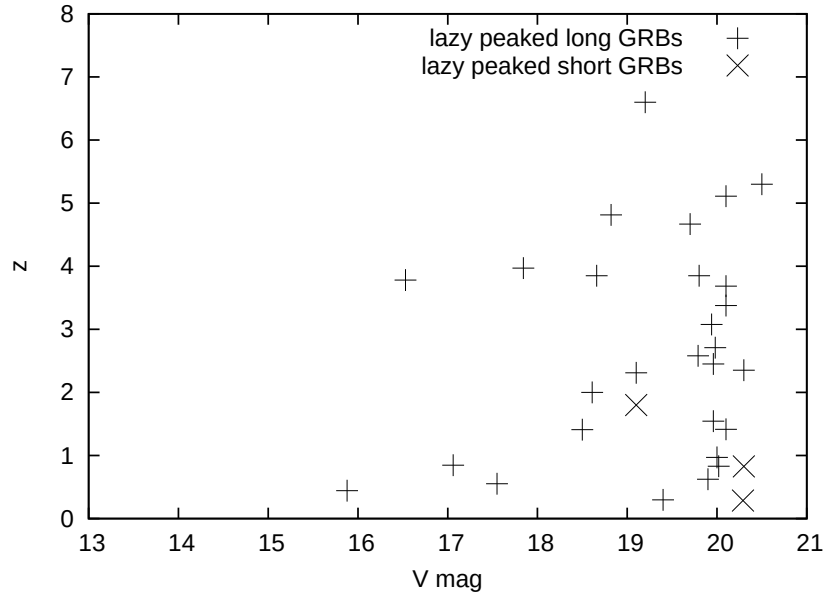

Figure 10.14: Lazy peaked gamma ray burst in the redshift - UVOT magnitude relation.

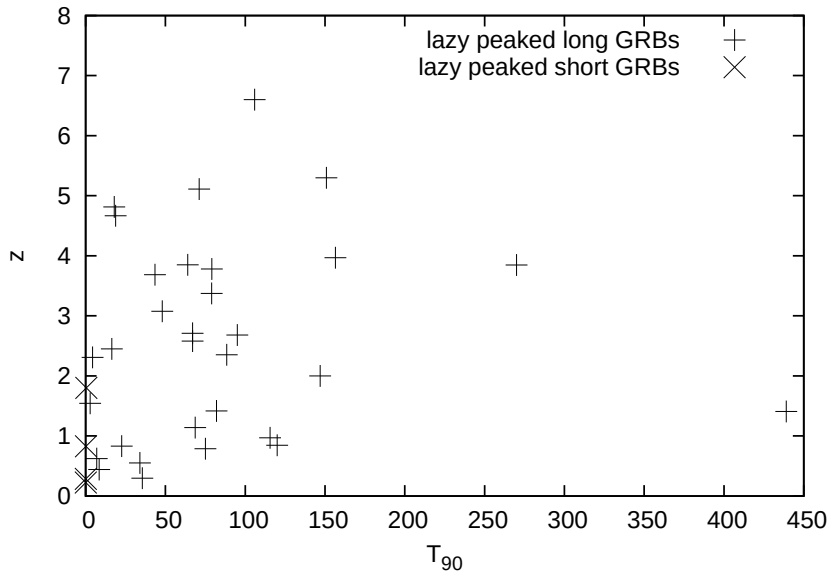

Figure 10.15: Lazy peaked gamma ray burst in the redshift - duration relation.

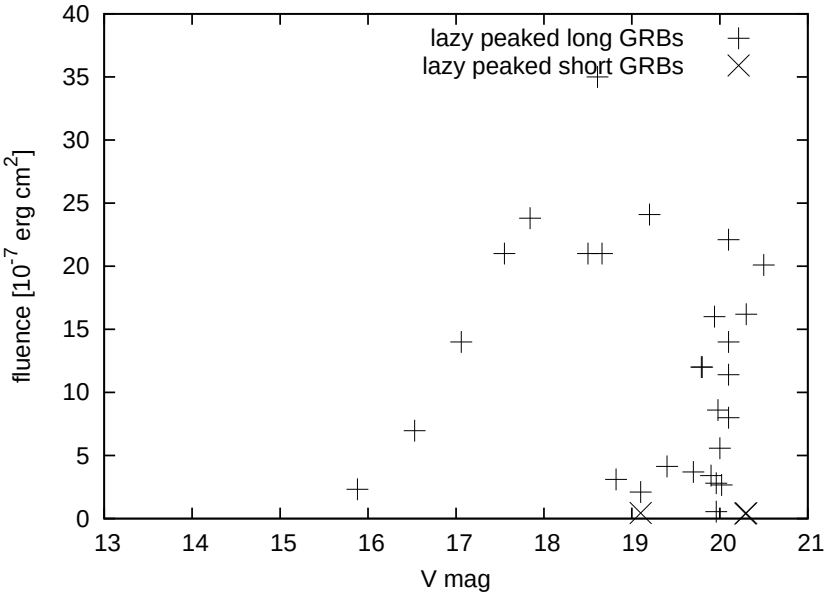

Figure 10.16: Lazy peaked gamma ray burst in the total fluence - UVOT magnitude relation.

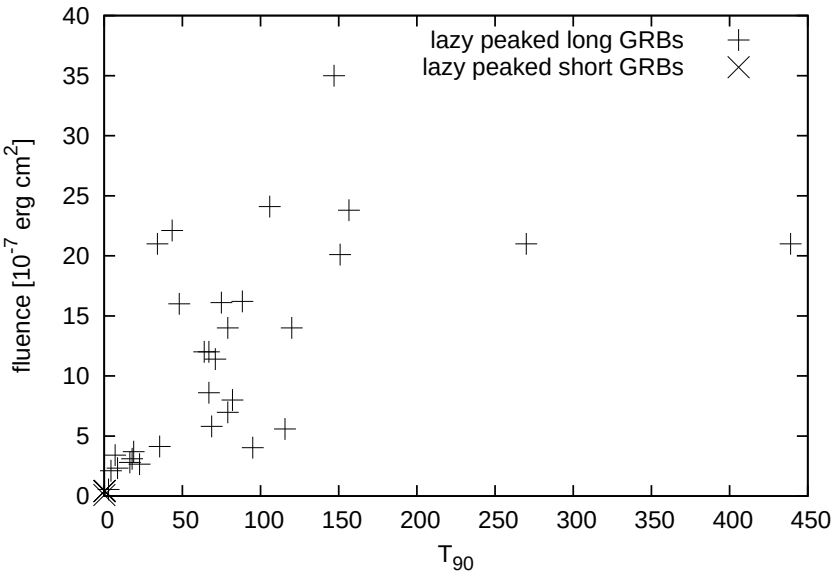

Figure 10.17: Lazy peaked gamma ray burst in the total fluence - duration relation.

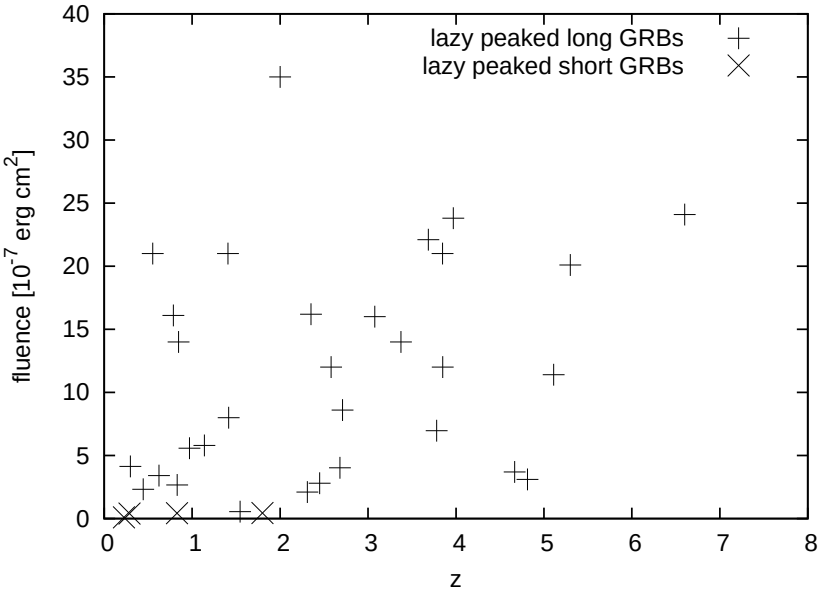

Figure 10.18: Lazy peaked gamma ray burst in the total fluence - redshift relation.

10.4 Correlations within the complex peaked group

The complex peaked GRBs appear to be not correlated at all. They are randomly distributed and the only thing one can estimate from the graphs is that they appear to be usually fainter in general (although the brightest GRBs detected by Swift are in this group). The absence of the grouping may be due to the fact that this group have the lowest number of the bursts.

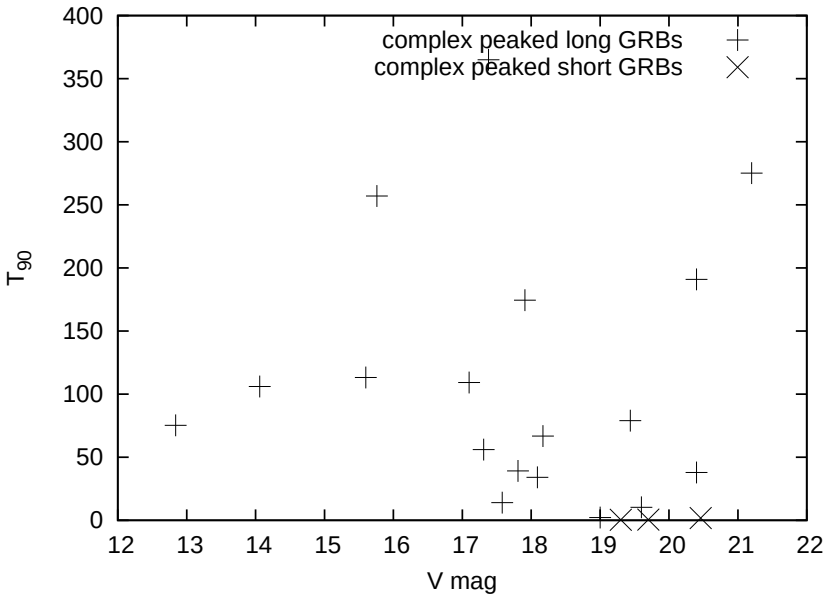

Figure 10.19: Complex peaked gamma ray burst in the duration - UVOT magnitude relation.

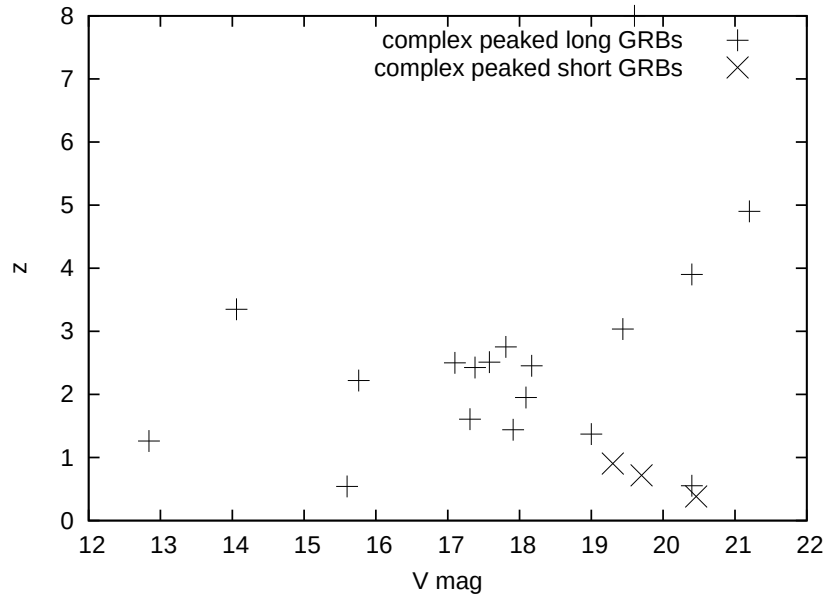

Figure 10.20: Complex peaked gamma ray burst in the redshift - UVOT magnitude relation.

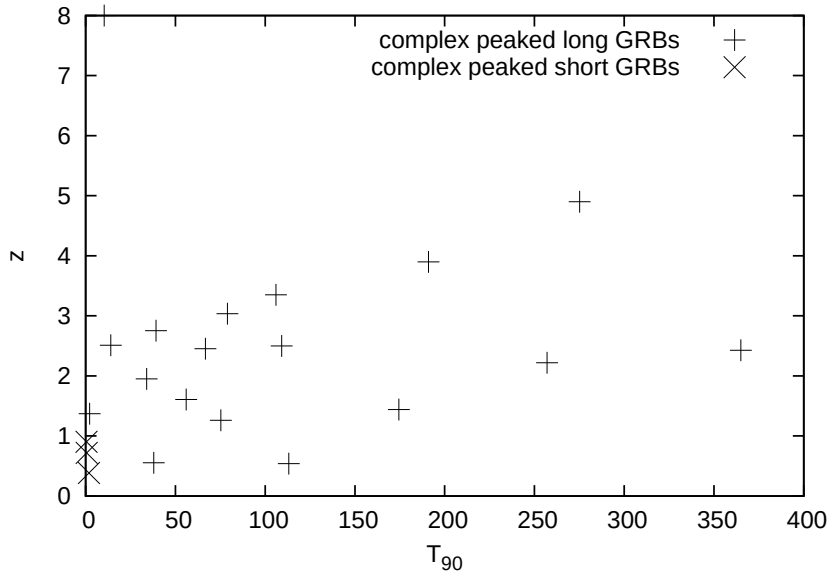

Figure 10.21: Complex peaked gamma ray burst in the redshift - duration relation.

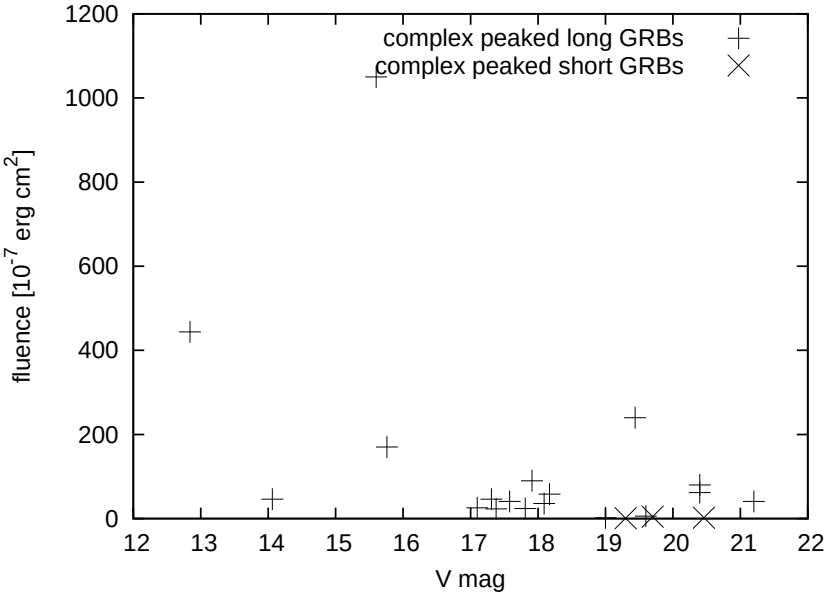

Figure 10.22: Complex peaked gamma ray burst in the total fluence - UVOT magnitude relation.

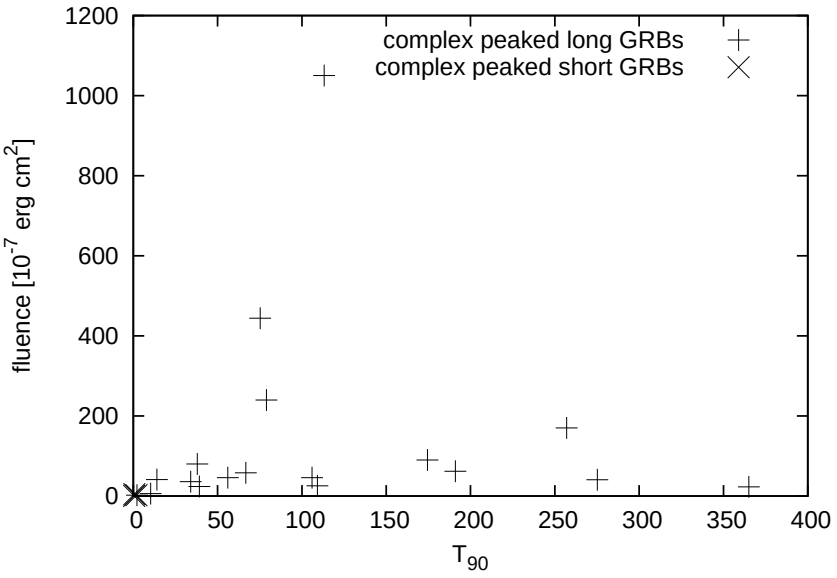

Figure 10.23: Complex peaked gamma ray burst in the total fluence - duration relation.

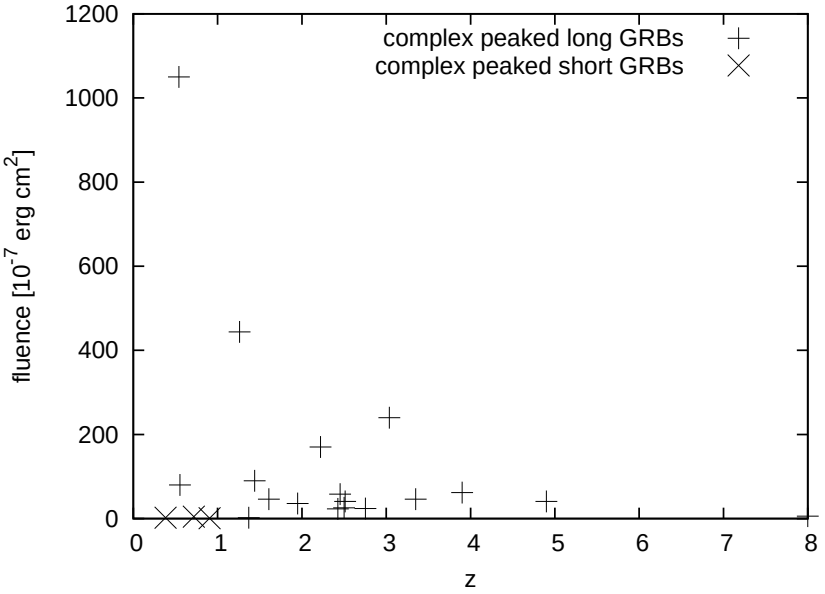

Figure 10.24: Complex peaked gamma ray burst in the total fluence - redshift relation.

10.5 Comparison of the groups

The following graphs are showing all groups plotted to one graph. It is a nice comparison of the newly proposed groups. All the relations mentioned in the previous sections are clearly visible. Also the clumping around the $z \sim 1$, as proposed by [6] is visible. Although the correlations seem to be detectable in the various groups in general, the whole sample of the GRBs do not appear to be correlated using parameters mentioned in this work. The graphs concerning fluence follow the study previously done by [42].

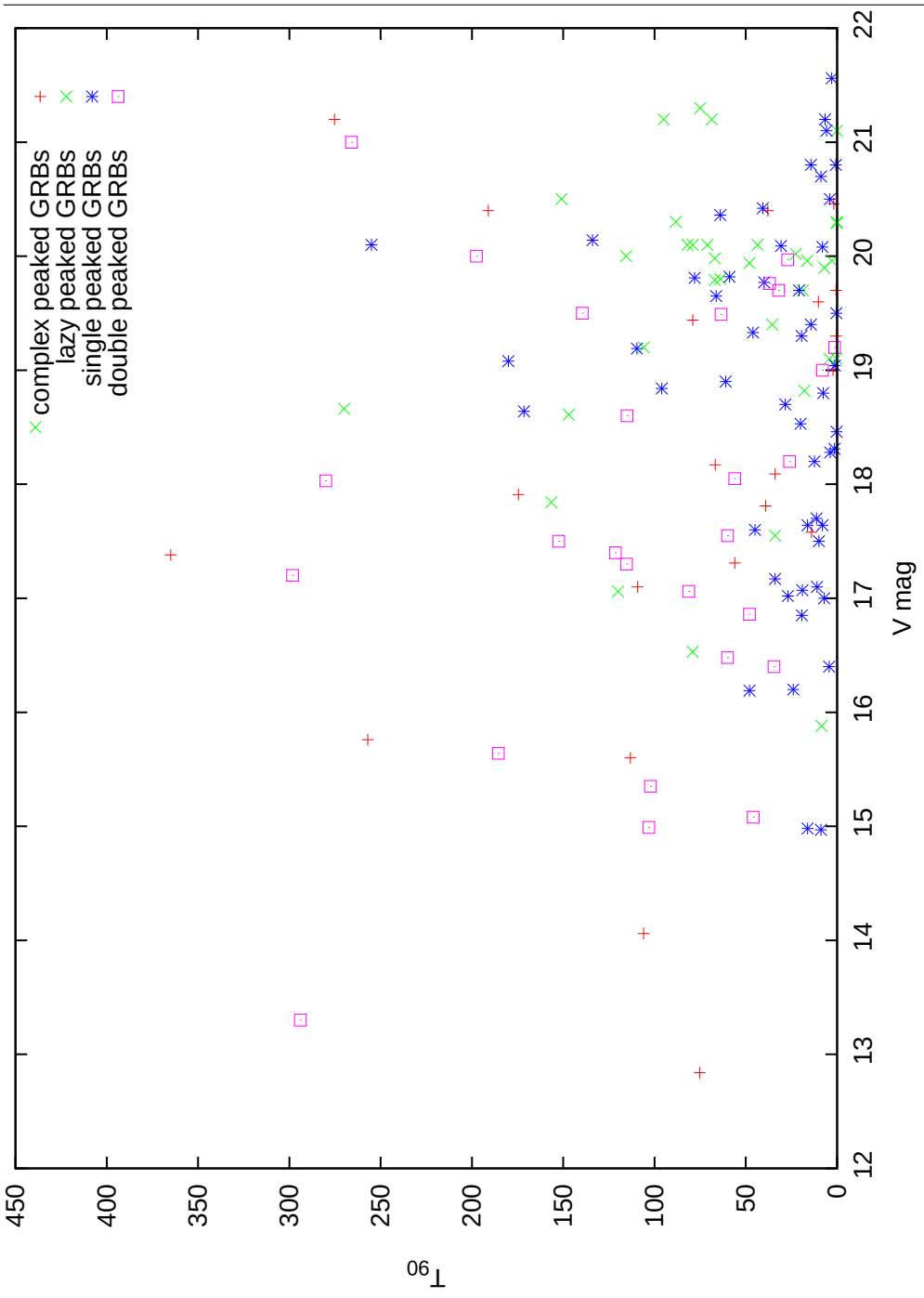

Figure 10.25: Redshift - time relation for all analyzed GRBs from the Swift sample.

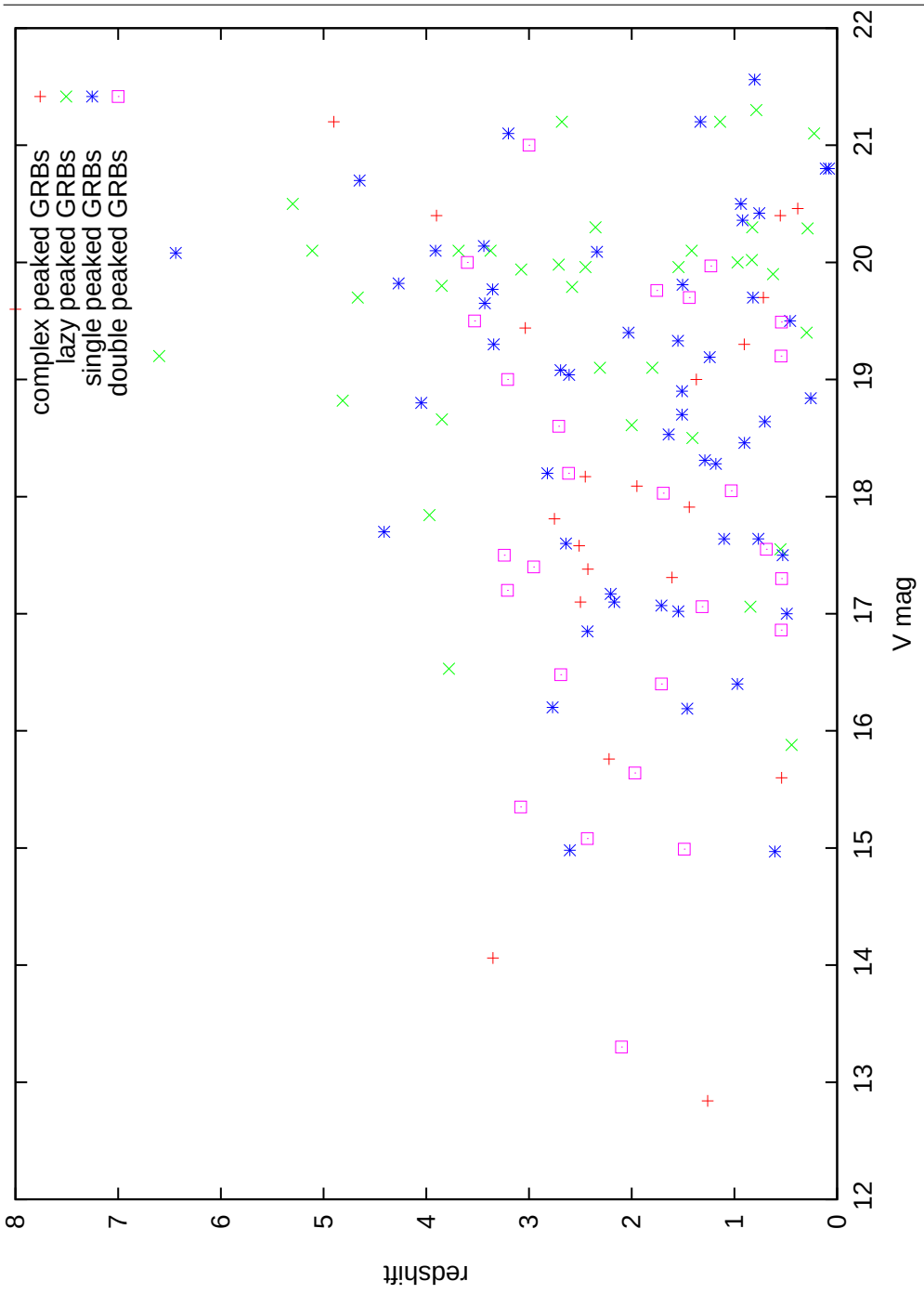

Figure 10.26: Redshift - duration relation for all analyzed GRBs from the Swift sample.

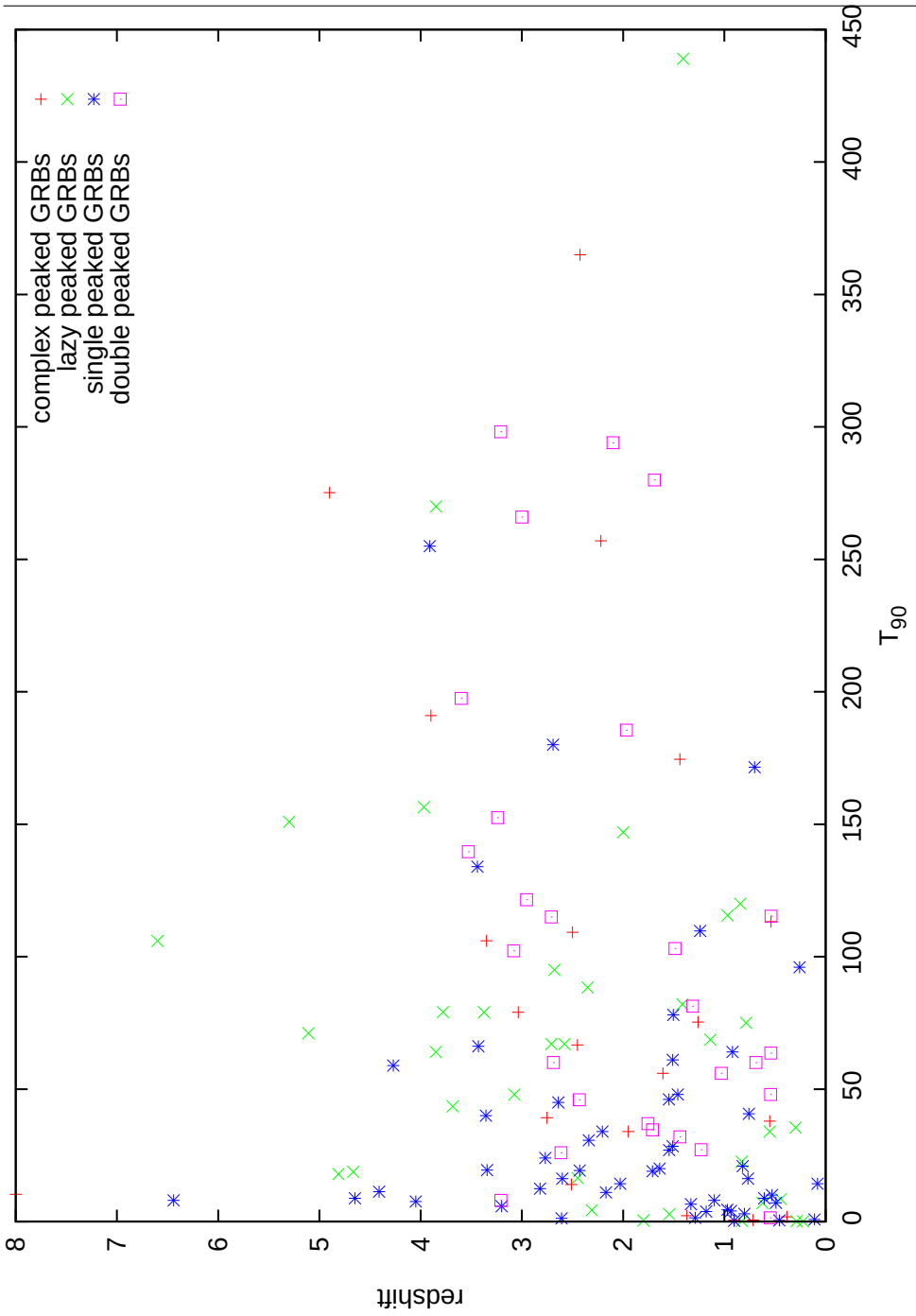

Figure 10.27: Redshift - duration relation for all analyzed GRBs from the Swift sample.

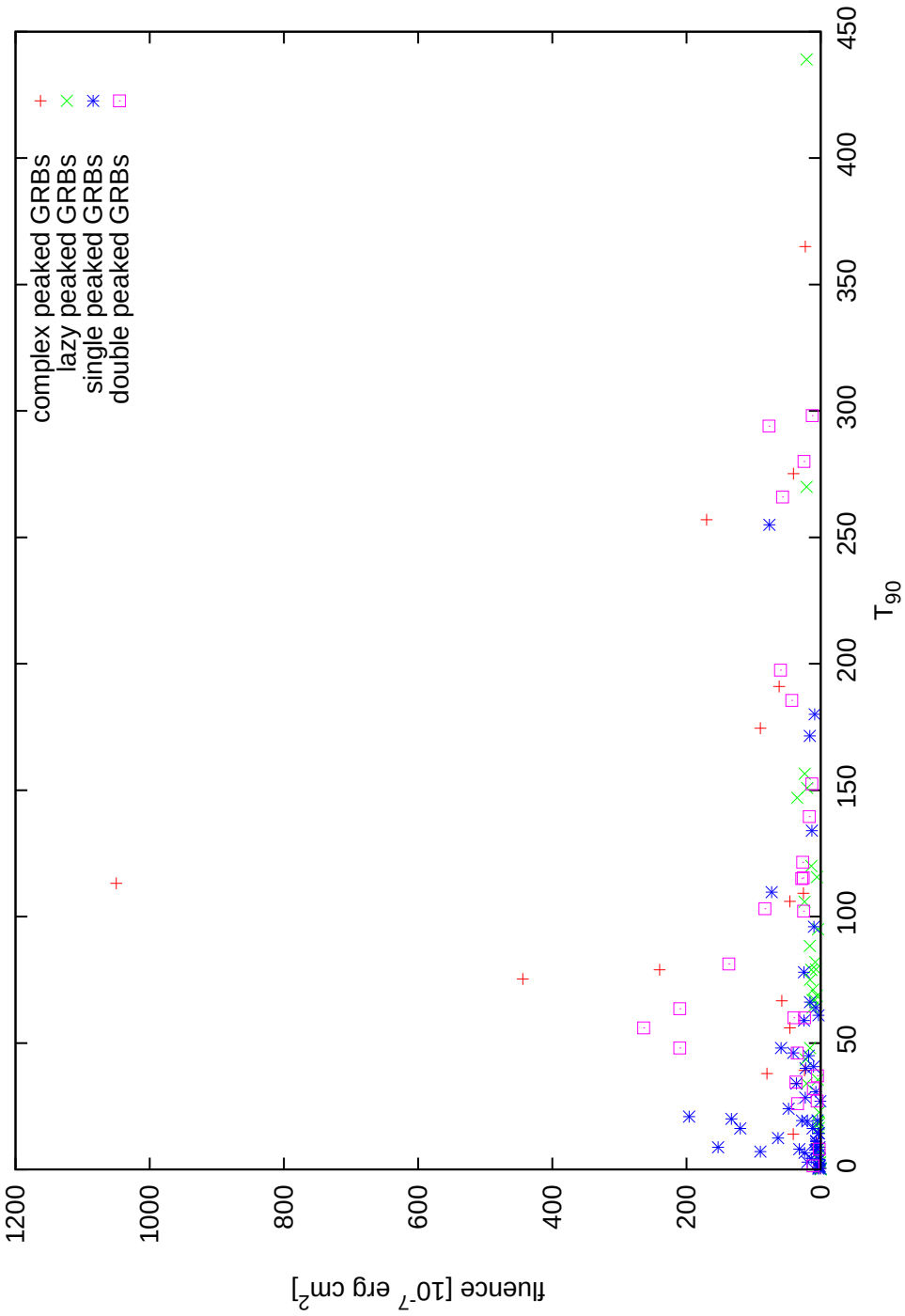

Figure 10.28: Total fluence - duration relation for all analyzed GRBs from the Swift sample.

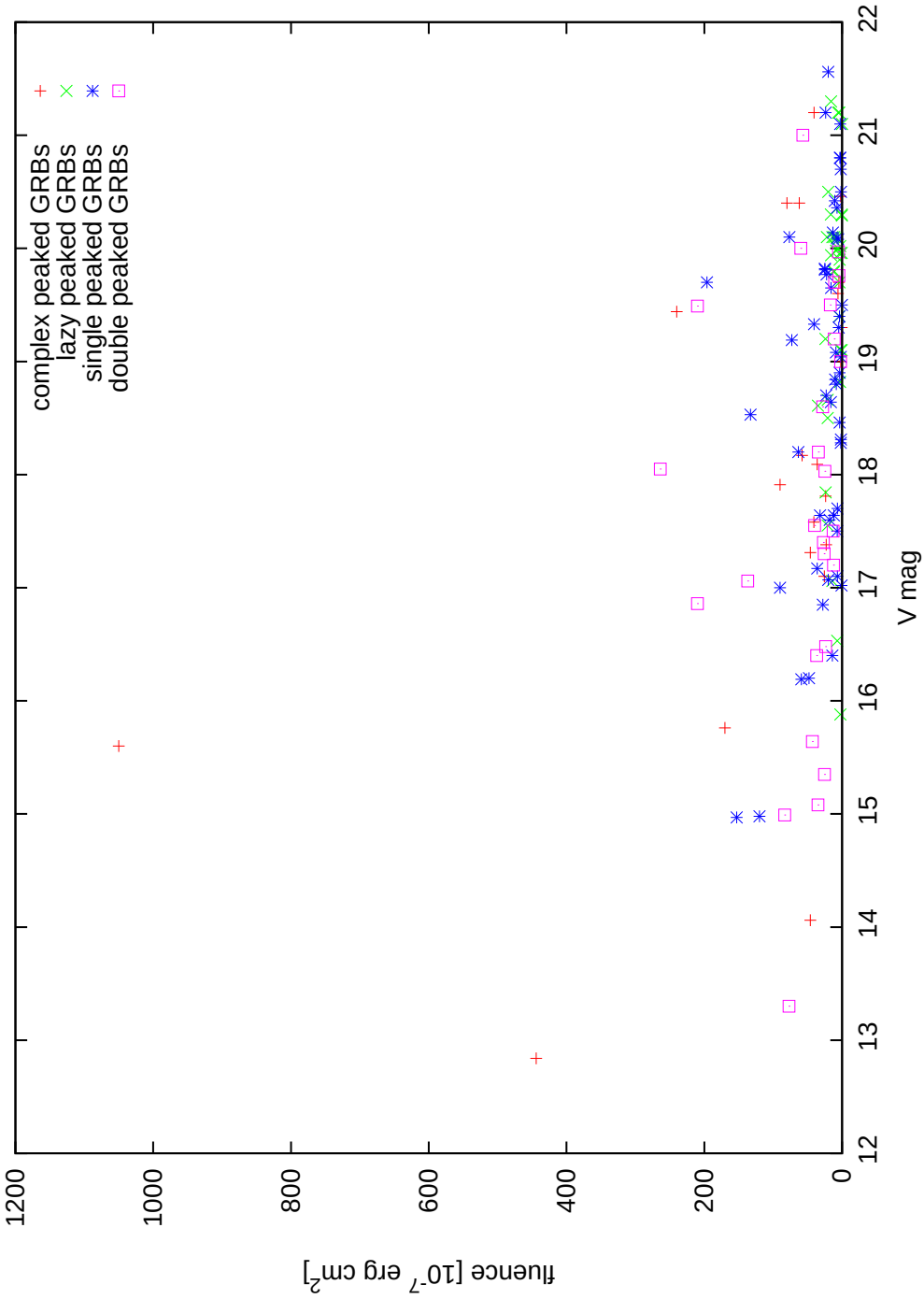

Figure 10.29: Total fluence - UVOT magnitude relation for all analyzed GRBs from the Swift sample.

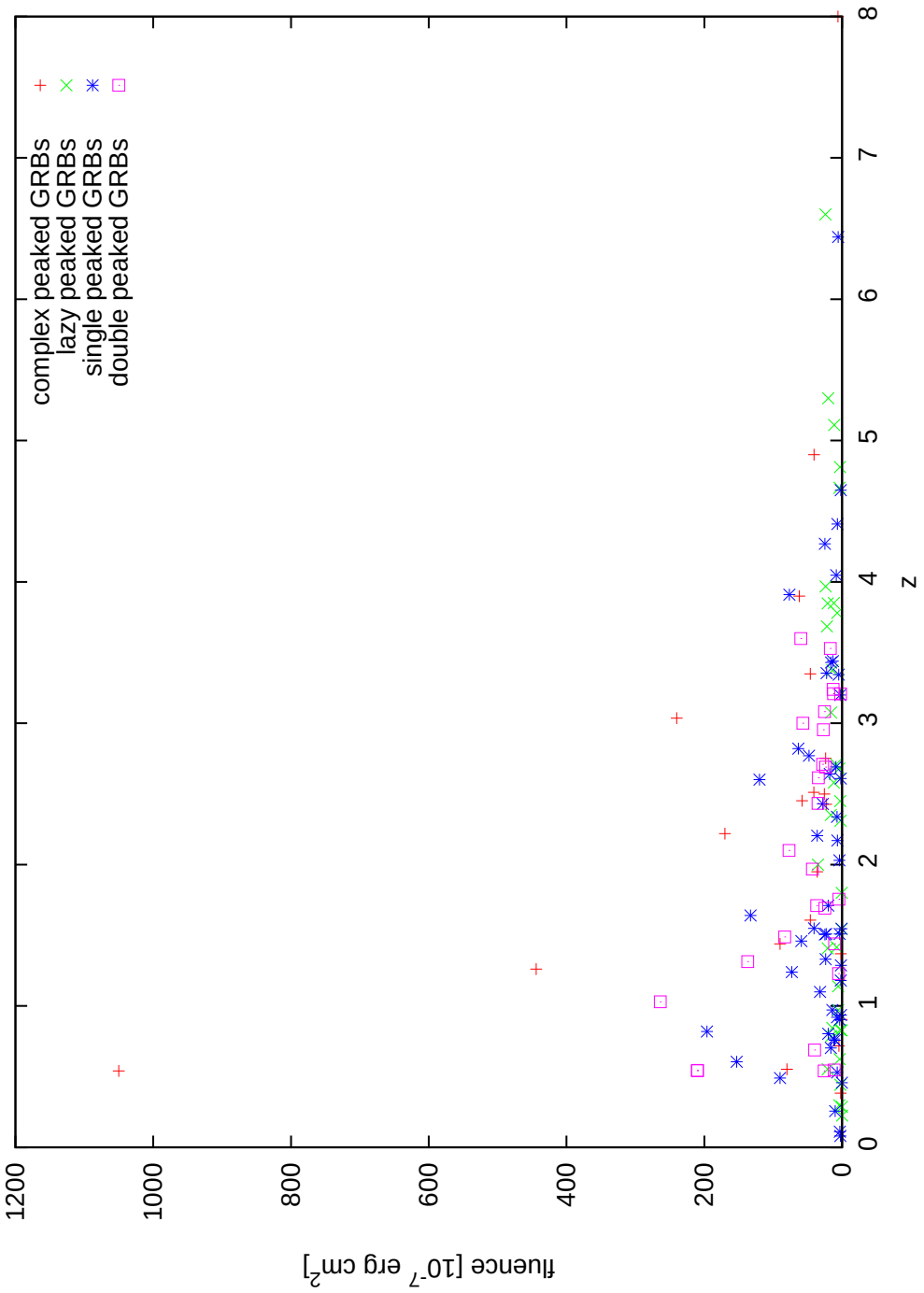

Figure 10.30: Total fluence - redshift relation for all analyzed GRBs from the Swift sample.

11 Conclusions

This work can be divided into three parts. The first part provided a short overview of the GRB science, mostly from the observational point of view. The most successful theory was briefly discussed and the basics facts describing the phenomena were introduced.

The second part is dedicated to the Swift satellite and the BAT data analysis, this part can be used as a simplified manual for the BAT data processing. Swift satellite is an ideal tool for this work since it is the only mission with so many GRBs with known redshifts and observational parameteres (UVOT V magnitude, fluence, duration). The other ongoing or past missions have only few bursts with known redshifts in the archive, as is discussed in Chapter 8.

The last part of the work is dedicated to the analysis of the processed data and the parameters obtained from Swift. The data were selected with emphasis on the known redshift as is mentioned above. Total number of 137 bursts was chosen. These bursts were divided into four groups according the geometrical features in the lightcurves. This is a newly proposed division originating in this work. The four groups are single peaked GRBs, double peaked GRBs, 'lazy' peaked GRBs and complex peaked GRBs. The observational parameters available from the Swift satellite are used in order to study possible correlation within this morphological groups.

The light curves can be divided into the proposed groups quite equally. The commonly recognized subgroups of the GRBs according the durations are highlited in the graphs, although the sample of short GRBs with known redshift seem to be quite small. This is thanks to the observational effects. Swift as well as the other missions is not very successful in catching the short GRBs, since they require a great deal of luck to be caught.

The results of this work follow the results proposed by [6], concerning the clumping of the short bursts around $z \sim 1$, which supports theory of the

origin of the short bursts in the neutron stars or the black holes mergers, discussed in Section 6.1 of this work. It is clearly visible in graphs 10.27, 10.9 and 10.4.

Another result concerning the dependence of the fluence on the redshift follows [42]. Cited paper as well as this work shows that it is not necesarilly true that the bursts with high redshifts have low fluences. Every proposed group follows the homogenous distribution of the fluences. It can be seen in 10.3, 10.1, 10.5, 10.9, 10.2, 10.11, 10.3, 10.17, 10.21, 10.4 and 10.23.

One of the results was quite surprising. The newly proposed group of 'lazy' GRBs exhibits a clumping around UVOT $\mathrm{mag_V} = 20$. It is noticeable on the graphs 10.3, 10.13 and 10.15. Those are equally distributed in the redshifts and fluences as can be seen in 10.13 and 10.15. The explanation of the geometrical phenomena may be caused by the fact the burst is slightly off the line of the sight or by the fact that the burst is dominated by the external shock model which is able to explain smooth curves as proposed by [48]. The explanation for this clumping is not clear, since the brightness in UVOT is redshift and fluence independent.

In general, no other correlations were found, as was expected in [19]. As can be seen from the graphs 10.25 and 10.26, the optically bright (in terms of UVOT) bursts do not exhibit the same behavior in the terms of morphology. As is discussed in Section 9.1, this expectation was build on the study of the RHESSI sample. There is also no indication of the third group of the intermediate GRBs [27] with $\mathrm{T_{90}} \sim 2$ s using this approach.

This work suffers from some problems caused by the observational constraints and selection effects. The light curves from the BAT are believed to be quite good, although mostly in the case of the 'lazy' GRBs, the S/N ratio is quite low, as can be seen i.e. in 9.3. The light curve appears to be not complicated at all but the minor changes can be lost in the noise. Another problem is encountered by the complex group which is very diverse, hence no correlations can be expected. Taken aside the proposed grouping, there is no significant correlation between the Swift GRBs detected in the selected sample.

Bibliography

[1] Amati, L. et al.: *Instrictic spectra and energies of BeppoSEX Gamma-Ray Bursts with known redshift*, A&A, 2002.

[2] Amati, L. et al.: *The $E_{\mathrm{p,i}}$-E_{iso} correlation in gamma-ray bursts: updated observational status, re-analysis and main implications*, MNRAS, 2006.

[3] BAT team: *The SWIFT BAT software guide* `http://heasarc.nasa.gov/docs/swift/analysis/bat_swguide_v6_3.pdf`, 2007.

[4] Barthelmy, S. D. et al.: *The Burst Alert Telescope (BAT) on the Swift MIDEX mission*, Space Science Reviews, 2005.

[5] Belobodorov, A. M.; Stern B.E., Svensson, R.: *Power density spectra of gamma-ray bursts*, ApJ, 2000.

[6] Berger, E. et al.: *A New Population of High-Redshift Short-Duration Gamma-Ray Bursts*, ApJ, 2007.

[7] Berger, E., Fong, W. J.: *The Galactic and Sub-Galactic Environments of Short-Duration Gamma-Ray Bursts: Implications for the Progenitors*, arXiv:0912.4142v1 [astro-ph.HE], 2009

[8] Bloom J. et al.: *Closing in on a short-hard burst progenitor: constraints from early-time optical imaging and spectroscopy of a possible host galaxy of GRB 050509b.*, ApJ, 2005.

[9] Briggs, M. S. et al.: *BATSE observations of the large scale isotropy of gamma-ray bursts*, ApJ, 1996.

[10] Campana, S. et al.: *Are Swift gamma-ray bursts consistent with the Ghirlanda relation?*, A&A, 2007.

[11] Carroll B. W., Ostlie D. A.: *An Introduction To Modern Astrophysics, (2nd edition)*, San Francisco : Pearson Addison-Wesley, 2007.

[12] Cavallo, G; Rees, M. J.: *A qualitative study of cosmic fireballs and gamma-ray bursts*, MNRAS, 1978.

[13] Cline, T. L. et al.:*Detection of a fast, intense and unusual gamma-ray transient*, ApJ, 1980.

[14] Cline, T. L. et al.:*Presice source location of the anomalous 1979 burst March 5 gamma-ray transiens*, ApJ, 1982.

[15] Colgate, S. A. et al.: *Prompt gamma rays and X-rays from supernovae*, CaJPS, 1968.

[16] Costa, E. et al.:*Discovery of an X-ray afterglow associated with the gamma-ray burst of 28 February 1997*, Nature, 1997.

[17] Daigne, F.; Mochkovitch, R.: *Gamma-ray bursts from internal shocks in a relativistic wind: a hydrodynamical study*, A&A, 2000.

[18] Doggett, J. B.; Branch, D.:*A comparative study of supernova light curves*, AJ, 1985.

[19] Fishman, G. J. et al.:*Overview of observations from BATSE on the Compton Gamma Ray Observatory*, A&A, 1993.

[20] Fenimore, E. E.; Epstein, R.I.; Ho, C.: *The escape of 100 MeV photons from cosmological gamma-ray bursts*, A&AS, 1993.

[21] Galama, T. J. et al.: *A hypernova model for the supernova associated with the gamma-ray burst of 25 April 1998*, Nature, 1998.

[22] Galama, T. J. et al.: *An unusual supernova in the error box of the gamma-ray burst of 25 April 1998*, Nature, 1998.

[23] Ghirlanda, G.; Ghisellini, G.; Lazzati, D.: *The collimationcorrected GRB energies correlate with the peak energy of their νF_ν spectrum*, ApJ, 2004.

[24] Ghirlanda, G. et al.: *Comments on "Are Swift Gamma-Ray Bursts consistent with the Ghirlanda relation?", by Campana et al. (A&A 2007)*, 2007arXiv0704.0234G, 2007.

[25] Ghirlanda, G.: *Gamma-ray bursts spectral correlations and their cosmological use*, 2007RSPTA.365.1385G, 2007.

[26] Hjorth J. et al.: *The optical afterglow of the short gamma-ray burst GRB 050709*, Nature, 2005.

[27] Horvth, I. et al.: *A new definition of the intermediate group of gamma-ray bursts*, A&A, 2006.

[28] Kitchin, C. R.: *Astrophysical techniques*, CRC press, 2009.

[29] Klebesadel, R. et al.: *Observations of gamma-ray burst of cosmic origin*, ApJ, 1973.

[30] Kobayashi, S.; Piran, T.; Sari, R.: *Hydrodynamics of a Relativistic Fireball: The Complete Evolution*, ApJ, 1999.

[31] Koshut T. M. et al.: T_{90} *as a Measurment of the Duration of GRBs*, AAS, 1995.

[32] Kouveliotou, C. et al.:*A 2.2 second period in the 1984 August 5 burst gamma-ray burst*, ApJ, 1988.

[33] Kouveliotou, C. et al.: *Identification of Two Classes of Gamma Ray Bursts*, ApJ, 1993.

[34] Leavitt, H. S.; Pickering, E. C.:*Periods of 25 Variable Stars in the Small Magellanic Cloud*, Harvard College Observatory Circular, 1912.

[35] Leloudas, G. et al.: *Do Wolf-Rayet stars have similar locations in hosts as type Ib/c supernovae and long gamma-ray bursts?*, A&A, 2010.

[36] Lestrade, J. P.: *The duration VS intensity diagram for a subset of PHEBUS gamma-ray bursts*, A&A, 1993.

[37] Lestrade, J. P.: *A new variability parameter for gamma-ray burst time profiles*, ApJ, 1994.

[38] Lithwick, Y.; Sari, R.: *Lower Limits on Lorentz Factors in Gamma-Ray Bursts*, ApJ, 2001.

[39] MacFayden, A. I.; Woosley, S. E.: *Collapsars: Gamma-ray bursts and explosions in 'failed supernovae'*, ApJ, 1999.

[40] Mazets, E. P. et al.:*Catalog of cosmic gamma-ray bursts from the KONUS experiment data. I.*, Ap&SS, 1981.

[41] Mazets, E. P.; Golenetskii, S.V.: *Cosmic gamma-ray bursts*, Ap&SS, 1981.

[42] Meszaros, A.; Řípa, J.; Ryde, F.: *Cosmological effects on the observed flux and fluence distributions of gamma-ray bursts: Are the most distant bursts in general the faintest ones?*, arXiv:1101.5040v1, 2011.

[43] Meszaros, P.; Laguna, P.; Rees, M. J.: *Gasdynamics of relativistically expanding gamma-ray burst sources - Kinematics, energetics, magnetic fields, and efficiency*, ApJ, 1993.

[44] Meynet, G; Maeder, A.: *Stellar evolution with rotation. XI. Wolf-Rayet star populations and different metallicities*, A&A, 2005.

[45] Paczynki, B.: *Gamma-ray bursters at cosmological distances*, ApJ, 1986.

[46] Panaitescu, A.; Meszaros, P.: *Radiative Regimes in Gamma-Ray Bursts and Afterglows*, ApJ, 1998.

[47] Prochaska, J. X. et al.: *The Galaxy Hosts and Large-Scale Environments of Short-Hard Gamma-Ray Bursts*, ApJ, 2006.

[48] Rees, M. J.; Meszaros, P.: *Relativistic fireballs - Energy conversion and time-scales*, MNRAS, 1992.

[49] Rees, M. J.; Meszaros, P.: *Relativistic fireballs and their impact on external matter - Models for cosmological gamma-ray bursts*, ApJ, 1993.

[50] Rees, M.J.; Meszaros, P.: *Unsteady outflow models for cosmological gamma-ray bursts*, ApJ, 1994.

[51] Sahu, K. et al.: *HST Observations of GRB 970228*, AAS, 1997.

[52] Sakamoto, T. et al.: *High Energy Transient Explorer-2 observations of the extremly soft X-ray flash XRF 020903*, ApJ, 2004.

[53] Sakamoto, T. et al.: *The First Swift BAT Gamma-Ray Burst Catalog*, ApJS, 2008.

[54] Savaglio S.; Glazebrook, K.; Le Borgne, D.: *GRB host Studies (GHostS)*, AIP, 2006.

[55] Stern, B. E.: *A stretched exponential law for average time history of gamma-ray bursts and their time dilations*, ApJ, 1996.

[56] Stern, B. E.; Svensson, R.: *Evidence for 'chain reaction' in the time profiles of gamma-ray bursts*, ApJ, 1996.

[57] Stern, B. E.; Poutanen, J.; Svensson, R.: *A complexity-brightness correlation in gamma-ray bursts*, ApJ, 1999.

[58] Vedrenne, G.; Atteia, J. L.: *Gamma-ray bursts The brightest explosions in the Universe*, Chichester: Springer Praxis publishing, 2009.

[59] Vink, J. S.; de Koter, A.: *On the metallicity dependence of Wolf-Rayet winds*, A&A, 2005.

[60] Woosley, S. E.: *Gamma-ray bursts from stellar mass accretion discs around black holes*, ApJ, 1993.

[61] Woosley, S. E.; Heger A.: *The progenitors stars of gamma-ray bursts*, ApJ, 2006.

[62] Adams, D.: *The Hitchhiker's Guide to the Galaxy*, Pan Books, 1979.

[63] Hudec, R.: personal correspondence.

[64] Nousek, J. A.: personal correspondence.

[65] Page, K.: personal correspondence.

[66] `http://swift.gsfc.nasa.gov/docs/swift/swiftsc.html`

[67] `http://heasarc.gsfc.nasa.gov/docs/cgro/index.html`

[68] `http://swift.sonoma.edu/about_swift/instruments/bat.html`

[69] `http://www.swift.psu.edu/xrt/`

[70] `http://www.swift.psu.edu/uvot/`

[71] `http://grb.web.psi.ch/`

Typeset in LaTeX 2_ε. The work used exclusively free software.